Halide perovskite nanocrystals for next-generation optoelectronics

*Maning Liu, Haichang Zhang, Dawit Gedamu, Paul Fourmont, Heikki Rekola, Arto Hiltunen, Sylvain G. Cloutier, Riad Nechache, Arri Priimagi, Paola Vivo**

Dr. M. Liu, Dr. H. Rekola, A. Hiltunen, Prof. A. Priimagi, Dr. P. Vivo
Faculty of Engineering and Natural Sciences, Tampere University, P.O. Box 541, FI-33014 Tampere, Finland
E-mail: paola.vivo@tuni.fi

Dr. H. Zhang
National and Local Joint Engineering Laboratory for Slag Comprehensive Utilization and Environmental Technology, School of Material Science and Engineering, Shanxi University of Technology, Hanzhong 723001, PR China

Dr. D. Gedamu, P. Fourmont, Prof. S. G. Cloutier, Prof. R. Nechache
École de Technologie Supérieure, Department of Electrical Engineering, 1100 rue Notre-Dame Ouest, Montréal (QC) H3C 1K3, Canada

Keywords: perovskite, nanocrystals, photophysics, photoluminescence, optoelectronic devices

Abstract

Colloidal perovskite nanocrystals (PNCs) combine the outstanding optoelectronic properties of bulk perovskites with strong quantum confinement effects at the nanoscale. Their facile and low-cost synthesis, together with superior photoluminescence quantum yields and exceptional optical versatility, makes PNCs promising candidates for next-generation optoelectronics. However, this field is still in its early infancy and not yet ready for commercialization due to several open challenges to be addressed, such as toxicity and stability. In this review, the key synthesis strategies and the tunable optical properties of PNCs are discussed. The photophysical underpinnings of this technology, in correlation with the most recent developments of PNCs-based optoelectronic devices, are especially highlighted. Our final goal is to outline a theoretical scaffold for the design of high-performance devices that can at the same time address the commercialization challenges of PNC-based technology.

1. Introduction

Over the past few years, halide perovskites (HPs) have generated extensive interest as a material of choice for various applications such as photovoltaics,[1–3] light-emitting diodes (LEDs),[4,5]

lasers,[6,7] and photodetectors (PDs).[8,9] Perovskite materials crystallize in an ABX_3 structure, where typically A = $CH_3NH_3^+$ (MA), $CH(NH_2)_2^+$ (FA), or Cs^+, B = Pb^{2+}, Sn^{2+}, X = Cl^-, Br^-, or I^-. They exhibit outstanding optoelectronic properties including high absorption coefficient, sharp band edge, tunable bandgap (400–800 nm), long diffusion length of charge carriers (~1 μm), and high charge-carrier mobility (1-10 cm^2 V^{-1} s^{-1}).[10–15] Recent reports using conventional single or bulk perovskite crystals as light absorbers have shown low-cost perovskite solar cells (PSCs) with power conversion efficiency (PCE) approaching 24 %[1] and perovskite-based LEDs (Pe-LEDs) with incident-photon-to-current conversion efficiency (IPCE) over 10 %.[16] Most of the works on perovskite-based optoelectronics have so far employed lead (Pb)-based, or in some cases Pb-free HPs,[17,18] in the form of bulk thin films, microcrystals, and single crystals.[19–21] Nevertheless, the research community has recently expressed a strong interest in developing perovskite materials in the nanoscale, triggered by the success of colloidal quantum dots (QDs) of conventional semiconductors (*e.g.* CdS, CdSe, CdTe, PbS, PbSe).[22] These so-called 'perovskite nanocrystals' (PNCs), having at least one dimension smaller than 100 nm per unit crystal cell, combine the outstanding optoelectronic properties of HPs with strong quantum confinement effects, resulting in additional tunability of such properties with the nanocrystal size. PNCs, prepared via facile and low-cost colloidal synthetic routes, display high emissive properties covering the whole visible and even the near-infrared (NIR) spectral range.[23] In contrast to other conventional semiconductor materials such as Si, GaAs, and Cd chalcogenides, HPs have mainly an ionic lattice.[4] Therefore, highly crystalline PNCs can be readily formed even at room temperature.[4,24]

PNCs often exhibit low trap densities and narrow-band emission with higher photoluminescence quantum yield (PLQY) compared to bulk or single crystals.[25,26] Hence, they could bring perovskite-based optoelectronic devices closer to their commercialization, once their main weaknesses of toxicity and low stability are addressed.[27,28] Synthesis, characterization, and applications of a wide set of PNCs have been intensively investigated

during the last few years, and the key results are summarized in several good reviews.[4,29–31] However, a comprehensive overview of halide PNCs, with special emphasis on their intriguing optoelectronic properties in relation to the emerging applications, is not yet thoroughly reported. We aim at bridging this knowledge gap by providing a deep analysis of the key photophysical properties of PNCs, such as optical properties, PLQY, and charge-carrier dynamics, and comparing them to those of the corresponding bulk perovskite materials. This in turn allows us predicting the root causes behind the poorer performance in device applications of PNCs with respect to the bulk films.

In Section 2 of this review, we summarize the main synthesis methods of PNCs, providing some possible strategies to address their current challenges and the toxicity aspects of PNCs technology.[32–37] Upon controlling the different synthesis approaches and the related dominant factors, including compositional ratio, type or amount of capping ligands, and reaction temperatures, PNCs with tunable nanocrystal sizes, dimensionalities (0D – 3D), and morphologies can be achieved.[38–44] In Section 3, we correlate the defect tolerance to several surface passivation techniques and to PNCs properties and stability as well. The key optoelectronic properties are discussed by focusing on several significant properties, mainly including size-dependent optical spectra, trap-state-related photoluminescence quantum yield (PLQY), and dimensionality-dependent time-resolved photoluminescence (TRPL). In Section 4, we provide an overview of the current use of colloidal PNCs in key optoelectronic devices, *i.e.* LEDs, solar cells, lasers, and PDs. Some other applications are also possible for PNCs in the fields of photocatalysis,[4][17] water splitting,[45] and waveguides,[46] but these have not been covered in this review.

We also highlight the importance of a deep understanding of PNCs photophysics as crucial criterion for the assessment of device performance, and as guidance for its future optimization. Finally, we provide our perspective to address the existing critical points of halide PNCs, by

outlining potential evolution trends. We hope that this work will promote new insights and further research studies to boost the development of PNCs for next-generation optoelectronics.

2. Synthesis Challenges

The facile synthesis of Pb-based hybrid (*e.g.* $MAPbX_3$, $FAPbX_3$) or fully inorganic (*e.g.* $CsPbX_3$) nanometer-sized perovskite crystals, combined with their excellent optoelectronic properties, has motivated huge research efforts on this technology in the latest years.[47,48] In this section, we will briefly introduce the mainstream synthesis methods, including the pre-synthetic (colloidal synthesis) and post-synthetic chemical transformations, together with their related challenges. Finally, we will discuss a key issue hindering the commercialization of PNCs technology, *i.e.* the Pb toxicity, and we will provide an overview of the possible solutions to achieve environmentally friendly PNCs.

2.1. Pre-synthetic chemical transformation (colloidal synthesis)

The easy formation of PNCs even at room temperature, as a consequence of their highly ionic nature, enables several possible approaches for the direct synthesis of hybrid or inorganic colloidal PNCs, among which the most common methods are ligand-assisted reprecipitation (LARP) and hot-injection.[47]

2.1.1. LARP and hot injection methods

The overall reaction mechanism of LARP method is summarized in **Figure 1a**. In LARP, the precursors and ligands are mixed together in a highly polar, such as *N*-dimethylformamide (DMF), where dissolution of the salts is complete. Then, a precise volume of this solution is dropped into a non-polar solvent, such as toluene or 1-octadecene, which initiates the PNC formation and the aggregation process starts (**Figure 1b**). The choice of the solvents and the addition of ligands are crucial to enhance the PNC stability. LARP is a low-cost and scalable approach originally proposed for the synthesis of hybrid organic-inorganic PNCs, and later extended to the synthesis of fully inorganic PNCs. The first solution-based and non-template synthesis of colloidal PNCs was established by Pérez-Prieto *et al.* in 2014.[41] By using organic

ammonium cations with medium-length alkyl chain (*e.g.* octadecylammonium) as capping ligands, stable (for at least 3 months) QDs in solution, with an average diameter of 6 nm, were obtained. This allowed the fabrication of thin films of these PNCs via spin-coating. Luminescent PNCs (both in colloidal solution and in films) were obtained, though their PLQY was only around 20 %.

Later on, the LARP technique was further optimized by Zhang's group, by replacing octylammonium bromide and octadecylammonium bromide ligands with n-octylamine (OA) and oleic acid (OAC) into the reprecipitation process.[36] PNCs with size of 3.3±0.7 nm were formed through the addition of the perovskite precursors containing lead halide (PbX_2, with X = Cl, Br, I) and organic halide salts (CH_3NH_3X, where X = Cl, Br, I) into a polar solvent such as DMF. Since halide salts generally exhibit good solubility in polar solvents but not in non-polar ones, the mixture precursor was subsequently added dropwise to a solution with non-polar medium as anti-solvent, *i.e.* toluene, promoting the formation and precipitation of brightly luminescent and color-tunable QDs. Their PLQY raised up to 70 %, significantly advancing the state-of-the-art.[41] Such an increase in the PLQY was attributed to the high exciton binding energy in these small-sized QDs and to their proper surface passivation. The ligands' role was also investigated in this work, indicating that OA contributed to control the kinetics of crystallization and the size of the formed PNCs, while OAC played a key role in suppressing the QD aggregation effects, and thus improving their colloidal stability.

Besides the capping ligands, the reaction temperature also affects the formation and the optical properties of PNCs. $MAPbBr_3$ perovskite QDs with size-tunable bandgap can be obtained by adjusting the anti-solvent's temperature to tailor the ligand-assisted reprecipitation process.[49] A bright emission with color change from blue to green was observed upon varying the temperature between 0 °C and 60 °C (cf. **Figure 1c**). This demonstrates that higher temperatures favor the formation of larger perovskite QDs due to the fast nuclear growth in hot reactions, similarly to conventional inorganic QDs such as PbS.[50] A facile LARP strategy at room

temperature for PNCs with tunable shape, from zero-dimensional spherical QDs to one-dimensional nanorods, two-dimensional nanoplatelets, and three-dimensional nanocubes (see **Figure 1d**), has been reported by Sun's group.[44] In this work, hexanoic acid and OA lead to spherical QDs, acetate acid and dodecylamine to 1D nanorods, OAC and OA lead to 2D nanoplates, while OAC and dodecylamine lead to 3D nanocubes.[44] The formation of the various-shaped PNCs with different organic acids and amines could be speculated by a classic micellar transition mechanism, which depends on the electrostatic and hydrophobic interaction with ions, the ligands, and the good and bad solvents.[51,52]

Compared to the LARP method, the so-called hot injection technique is an alternative synthesis route based on an ionic metathesis approach. The hot injection method does not involve polar solvents but requires a high synthesis temperature (up to 250 °C) and inorganic molecular precursors that are stable at that temperature. Typically, a cation (in the form of Cs-oleate for Cs^+ or methylamine for MA^+) is quickly injected into a solution containing a metal halide salt (*e.g.* PbX_2) and capping ligands (*e.g.* alkyl chain amine and acid) at high temperature, resulting in the formation of ternary halide PNCs upon the rapid salts metathesis reaction (see **Figure 1f**).[47] The overall reaction mechanism of the hot injection method is illustrated in **Figure 1e**. The first fully inorganic $CsPbX_3$ PNCs achieved by hot injection approach were reported by Protesescu *et al.*[35] During the ionic metathesis reaction, the fast nucleation and nanocrystal growth form a cubic shape with tunable lateral size (between 4 – 15 nm) by the reaction temperature. In addition, by adjusting the halide composition, size-tuned emission ranging over the entire visible spectral region (**Figure 1g**), with PLQY between 50 – 90%, was observed. Hot injection often allows achieving better phase purity of PNCs compared to LARP, mainly because the high reaction temperature allows dissolving the impurities. Recently, Pan *et al.* reported that the length variation of carboxylic acids and amines, as well as the reaction temperature, significantly affect the size and the shape of the PNCs.[53] The reduction of the

carboxylic acid and amines lengths results in a monotonic size increase of the formed PNCs, while changing the reaction temperature will generate differently-shaped PNCs.

Since conventional LARP and hot injection suffer from synthesis limitations, *i.e.* the use of inorganic salts (*e.g.* PbX_2) with fixed molecular ratio, it is not possible to flexibly tune the amount between the reaction species including lead and the halide salt complex. To address this drawback, very recently, a new colloidal route was developed, where the halide source and the lead salt are separated by the injection of benzoyl halides as halide precursors into the lead precursor. Such modified LARP employs the direct injection of benzoyl halides into a solution containing metal cations at a desired temperature, thus allowing the release of halide ions and the nucleation and growth of metal halide PNCs (**Figure 1h**).[54] The benzoyl halides might also be changed into other stable acyl halide molecules. With this approach it is possible to independently tune the amount of both cations and halide precursors in the synthesis. The resulting nanocrystals exhibited nearly cubic morphology, very high phase purity, narrow emission line width, high PLQY (～92 %), and good air stability for weeks without any post-synthesis treatment.[54] It should be noticed that, for $CsPbCl_3$ NCs prepared with this approach, lower amounts of benzoyl chloride will result in a weak PL emission. For instance, when using 0.6 mmol of benzoyl chloride and 0.2 mmol of the Pb precursor, NCs with relatively low PLQY (< 10 %) are obtained.

LARP and hot injection are the most common methods to synthesize organic-inorganic or fully inorganic PNCs. The main advantage of LARP is that the reactions can be performed at low temperatures (under 100 °C) as well as in ambient conditions. However, its drawback is that the existing polar solvents could dissolve the PNCs during purification. As regards to hot injection, the main advantage is that the lack of polar solvent allows easier control of the PNCs shape compared to LARP, while its main inconvenient is the need of high reaction temperature and inert atmosphere. In addition to the above-discussed colloidal synthesis approaches, recently other facile routes for colloidal PNCs preparation have also been developed, such as

one-pot reaction,[4,32] ultrasonic method,[33] microwave-assisted synthesis,[34] self-patterning,[55] and ball milling.[37] In this review, we are not going to discuss these methods further, but refer to refs. [30,46] for a comprehensive overview of the alternative synthetic approaches.

2.2 Post-synthetic transformations

PNCs combine the electronic and optical versatility of ionic inorganic solids with the synthetic versatility and tunability of covalent organic molecules. Their multicomponent crystalline structures, incorporating a wide array of metals, ligands, and organic molecules, can be synthetically fine-tuned to accommodate diverse target technologies (*e.g.* stoichiometry of halides and ligand exchange) through different post-synthetic transformation approaches.

2.2.1. Ion (halide anion or cation) exchange reactions

The high ionicity and the structural instability of PNCs make ion exchange reactions possible, which in turn allows easy tuning of the nanocrystals optical properties.[4] In fact, the emission spectra of PNCs can cover the whole visible spectral region, including even the NIR range, and the optical band gap can be adjusted accordingly (**Figure 2b**).[56] The tuning strategy for optical spectra will be discussed in detail in Section 3. It has been reported that, by adding the $MAPbBr_3$ PNCs into MACl- or MAI-dissolved isopropyl alcohol (IPA) solution, mixed halide PNCs (*e.g.* $MAPbBr_{3-x}Cl_x$ or $MAPbBr_{3-x}I_x$) can be successfully obtained (see the mechanism of the anion exchange in **Figure 2a**).[56] Since the solubility of $MAPbCl_3$ is higher than that of $MAPBI_3$ in IPA, the anion exchange between Br^- and Cl^- is significantly faster than between Br^- and I^-. A halide anion exchange reaction has been employed also for fully-inorganic PNCs by using different halide precursors, *i.e.* tetrabutylammonium halides (TBA-X), octadecylammonium halides (ODA-X), oleylammonim halides (OLAM-X), and lead halide salts (PBX_2). In the case of TBA-X, the halide exchange reaction only works from I^- to Br^- or from Br^- to Cl^-, while the reverse exchange does not work. However, the anion exchange is reversible for the other halide precursors (*i.e.* ODA-X and OLAM-X, **Figure 2c**).[57] This is due to the hard/soft acid/base interactions. Lyophilic quaternary TBA cation is a soft acid that prefers binding to softer halide

ions. The competing transformation from TBA-Br to TBA-Cl is not favored, as Br^- ions are softer than Cl^-, and thus prefer remaining associated with TBA. The same reasoning justifies the difficulty in exchanging Br^- ions in $CsPbBr_3$ NCs with I^- ions coming from TBA-I. In addition, the large difference in ionic radii between Cl^- and I^- anions explains why the direct exchange between Cl^- and I^- anions involves a structural stress on the perovskite lattice, which results in serious degradation of the nanocrystals. Other studies on the halide anion exchange have also been reported, such as halide exchange in solid phase,[58] in the forms of nanorod arrays,[59] nanowires[60] or nanocubes,[61] photoinduced anion exchange,[62] and gaseous hydrogen halides as the halide precursors.[63]

While halide anion exchange has already been investigated, studies on post-synthetic cation exchange in PNCs are quite rare. Stam *et al.* synthesized $CsPbBr_3$ PNCs, and subsequently exchanged Pb^{2+} cations with several other covalent cations, thus obtaining $CsPb_{1-x}M_xBr_3$ PNCs ($M = Sn^{2+}$, Cd^{2+}, and Zn^{2+}; $x \leq 0.1$).[64] The cation exchange induced a blue shift in the absorption and emission spectra, while preserving a high PLQY and narrow emission band-width. They assigned the blue-shift in the optical spectra to the contraction of the PNC lattice, leading to the shrinkage of Pb-X bonds or, in other words, to the increase of the Pb and Br orbitals interaction (**Figure 2d**). Protesescu *et al.* also demonstrated the partial or complete exchange at A-site cations (*e.g.* Cs^+ with FA^+ or MA^+, and in reverse).[65] The cation exchange reactions were performed in toluene solution containing $FAPbI_3$ NCs and Cs-oleate precursor (or $CsPbI_3$ NCs and FA-oleate precursor) to form $FA_xCs_{1-x}PbI_3$ NCs. Cation exchange could play an important role in reducing or even eliminating the toxicity of perovskite through lead replacement with low- or non-toxic elements such as Sn, Cd, and Zn. In addition, cation exchange could tune the PNCs' properties, namely the absorption or emission spectra, the band gap, and PLQY. The stability of the PNCs might be also improved through the cation exchange from hybrid organic-inorganic PNCs to fully inorganic PNCs.

Ion exchange reaction is a simple and effective approach to tune the optical properties of PNCs, such as leading its emission spectra covering the whole visible spectral region, enhancing its PLQY, and adjusting its optical absorption spectra. In addition, this technique can easily adjust the band gap of the PNCs to make it suitable for different applications such as LEDs, solar cells, and PDs.

2.2.2. Crosslinking reactions

Crosslinking refers to the process of forming ionic bonds (*e.g.* covalent or monovalent bonds) to connect two or more molecular chains. Once the materials are crosslinked, their chemical and physical properties are changed with respect to the starting materials. Interconnecting the PNCs to form crosslinked ones can not only enhance the perovskite stability and its tolerance towards humidity, but also tune PNCs properties, such as solubility and electroluminescence. Li *et al.* utilized butylphosphonic acid 4-ammonium chloride to be coated on a PNC film, by connecting the neighboring PNCs via hydrogen bond (N-H…I and P-OH…I) (**Figure 2e**). [61] The resulting crosslinked PNC film exhibited enhanced stability, uniform surface coverage, stronger moisture resistance, and red-shift in optical absorption compared to the non-crosslinked ones. The length of the alkyl chain connecting the neighboring PNCs is paramount to achieve effective crosslinking: a too long or too short alkyl chain can hinder the crosslinking, and accordingly decrease the PNC performance.

Hydrogen bond is a weak chemical bond, which could be decomposed at high temperature.[66,67] Hence, by replacing the hydrogen bonds with covalent bonds to form crosslinked PNCs, more promising optoelectronic properties could be gained. One example is the addition of trimethylaluminum (TMA) to $CsPbX_3$ PNCs to induce crosslinking reaction.[63] In this process, TMA first reacts with the carboxylate and amino groups of the ligands, adjacent to the PNCs, and forms intermediates. Subsequently, when exposing the intermediates to ambient conditions, crosslinked PNCs based on covalent bond are formed (**Figure 2f**). As a result, the crystal spacing is increased from 1.6 nm of the non-crosslinked PNCs up to 1.9 nm of the crosslinked

ones, leading to higher electroluminescence and more than one order of magnitude enhancement in external quantum efficiency (EQE) of the device. Later, Palazon *et al.* employed X-ray irradiation on the PNCs, inducing the alkyl chain interaction to form C=C bond crosslinked $CsPbX_3$ NCs (**Figure 2g**). The crosslinked PNCs were insoluble in toluene, while non-crosslinked NCs could be easily dissolved in this solvent. Crosslinking reaction transformation of the ligand shell improved the stability of the film and resulted in the insolubility of the exposed regions in toluene, which caused instead complete dissolution of the unexposed regions. Thus, crosslinking reaction could be used for lithography applications and enable the fabrication of stable and strongly fluorescent patterns over millimeter scale areas.[64] The crosslinking technique can not only enhance the PNCs stability and solubility, but can also adjust their optical properties, which is surely favorable for various optoelectronic applications.[63]

2.3 Towards environmental-friendly PNCs

The rapid development of PNCs for optoelectronics has been leading to impressive results, considering that PNCs have been developed to date for less than a decade. However, the toxicity of traditional Pb-based PNCs is a critical problem that makes this technology still not ready for commercialization.[66] This has recently driven an intense research worldwide towards environmentally friendly and chemically-robust Pb-free perovskite bulk materials, as well as nanocrystals.[4,67–70] Nevertheless, the reported Pb-free PNCs perform still poorly when compared to Pb-based ones.[71–73] Therefore, it is paramount to identify new Pb-free materials with high performance, and to enhance the performance of the reported ones. Density functional theory (DFT) offers a valid support in screening potential candidates for efficient molecular designs, mostly relying on bandgap and thermodynamic stability predictions.[70,74,75] More recently, also machine learning techniques have been successfully combined with DFT to accelerate the discovery of novel Pb-free perovskites with suitable characteristics.[76] The selection criteria when searching for elements to replace Pb in ABX_3 have been discussed in

several works, namely the defect tolerance mechanism, evidenced in materials whose electronic properties depend on the two electrons in the outermost s orbital of Pb^{2+} (*i.e.* 6s2), the octahedral factor, the bandgap, and the material stability.[68,76–78] In the following, we briefly assess the state-of-the-art on Pb-free PNCs, with an overview of the elements typically chosen to replace Pb. In **Table 1**, more detailed information on key selected Pb-free PNCs can be found.

The first and most straightforward approach consists of the replacement of Pb^{2+} with an isovalent cation such as tin $(Sn)^{2+}$or germanium $(Ge)^{2+}$.[15] Sn is the most well-known and promising candidate, since it affects the electric conductivity dramatically,[79] leading to the best performance in solar cells to date.[80] However, its drawbacks of poor stability and debatable toxicity[81] render Sn an unideal substitute of Pb in PNCs.[82] PNCs based on Ge^{2+}, a defect-tolerant semiconductor in which both s and p electrons hybridize to form the valence and conduction bands, do exhibit bright emission.[48] Unfortunately, such PNCs are also highly unstable. Furthermore, Ge^{2+} is not attractive from cost-effectiveness point of view, being a fairly rare chemical element. Finally, most of the Ge-based PNCs have larger bandgaps than their Pb-analogues, and their conductivity is poor due to the lone-pair effect.[4] Based on the above considerations, Ge-based halide perovskites have not received significant attention as light harvesters and have not found practical applications.

Ternary metal-halide materials including a trivalent metal ion (bismuth, Bi^{3+}), with similar electronic properties (because of the same 6s2 configuration) as Pb, have $A_3Bi_2X_9$ configuration, *e.g.* $(CH_3NH_3)_3Bi_2X_9$[83] or $Cs_3Bi_2X_9$.[69,84,85]. Antimony (Sb) is another element with low toxicity, belonging to the same column with Bi in the periodic table. PNCs with $A_3Sb_2X_9$ configuration have been also exploited. While the trigonal and orthorhombic phases of bulk $Cs_3Sb_2Cl_9$ have been investigated for more than 40 years,[86,87] the $Cs_3Sb_2X_9$ PNCs have only recently been explored. Examples of $(CH_3NH_3)_3Sb_2I_9$, $(NH_4)_3Sb_2I_xBr_{9-x}$, and $Cs_3Sb_2I_9$ PNCs obtained via noncolloidal routes have been reported.[88–90] More recently, solution phase synthesis of $Cs_3Sb_2X_9$ (X = Cl, Br, I) quantum dots has been also demonstrated.[91] These

materials have good stability, as suggested by Goldschmidt tolerance factor.[73,92,93] Additionally, the similarity of electronic configuration of $Cs_3Sb_2X_9$ with the organolead halide PNCs hold promise as interesting lead-free PNCs for optoelectronics.

The heterovalent replacement of two divalent Pb^{2+} ions with one monovalent (M_1^+) and one trivalent (M_2^{3+}) metal cation provides an alternative approach to overcome the toxicity of the traditional Pb-based perovskites, *i.e.* with the so-called double perovskites (DPs, structure $A_2M_1^+M_2^{3+}X_6$) materials. To shed some light on the thousands unexplored possible DP structures, it is paramount to identify and demonstrate new strategies to combine theoretical calculations and simulations, machine learning techniques, and laboratory prototypes to identify the most suitable materials according to their bandgap and thermal/environmental stability. Most relevant examples of published DPs include those where M_1^+ is Ag^+, Au^+, or Cu^+, and M_2^{3+} is Bi^{3+}, In^{3+}, or Ga^3. Unfortunately, most of the reported double PNCs have indirect bandgap. This implies weak oscillator strengths for optical absorption and for radiative recombination,[94] therefore being not ideal for *e.g.* photovoltaic or LED applications.

3. Optoelectronic properties

Compared to bulk or single crystals, PNCs exhibit enhanced optical and electronic properties as a consequence of their high surface-to-volume ratio, facile processability, and versatile functionalization.[95] Controlling the structure is very crucial for PNCs, since their shape and size affect the optoelectronic properties. Particularly, when the size (in the range 1–100 nm) of the nanocrystals is smaller than the Bohr exciton radius, the quantum confinement effect is induced.[43] Several different strategies have been employed for the formation of PNCs with diverse structures by tuning the synthesis conditions, as mentioned in the previous section. In addition, the concept of surface passivation, *i.e.* the use of capping ligands or functional groups on the surface of PNCs to passivate the surface or trap states, can also be utilized to tailor their properties and stability. In this section, based on the review of the most recent related works, we report about Pb-based and Pb-free PNCs in different dimensions (0D-3D), with a focus on

their distinct optoelectronic and photophysical properties, mainly including tunable optical properties, time-resolved studies, and bandgap engineering for suitable device applications.

3.1 Defect tolerance and surface passivation

One of the most attractive and well-known characteristics of PNCs is their high tolerance to different types of defects such as vacancies, surface states, and grain boundaries. This defect-tolerant nature is typically intrinsic, mainly attributed to the PNCs' electronic band structure, and to the nature of the valence band maximum (VBM) and conduction band minimum (CBM). The VBM has antibonding features, and the CBM is stabilized by the strong spin-orbit coupling.[96–98] The comparison between the defect tolerance mechanism in PNCs and in traditional metal chalcogenide nanocrystals is shown in **Figure 3a**.[29] In general, the defect states of PNCs are formed within the VBM or CBM rather than the bandgap, as it is for most of the conventional semiconductors. Thus, the bandgap of PNCs is nearly free of trap states and electronically clean. As a result, PNCs display intrinsically high luminescence, without the need of additional electronic surface passivation. However, as PNCs are more ionic than conventional semiconductor QDs (such as CdSe and CdS), the interactions with capping ligands are also more ionic and labile.[4,24] In fact, due to their electrovalent bond characteristics, luminescent PNCs are easy to synthesize, but also easy to be decomposed during the purification process (**Figure 3b**), which means that their chemical structure and optical properties can be easily changed.[4,48] As one example, when adding a polar solvent to purify $CsPbBr_3$ PNCs, they lose their surface ligands.[99] In this regard, surface ligands, *i.e.* molecules that bind to the surface, are an essential component of PNCs and should be carefully selected, since they influence their optical and chemical properties. Surface passivation is therefore still an important technique to enhance the stability and optical properties of PNCs.

So far, the surface chemistry of the ligands of halide PNCs mainly refers to alkyl-chain ligands bound to the nanocrystal surface via amino, carboxylate, or phosphonate groups. The combination of ligand types and PNCs stoichiometry can generate different binding motifs,

which play a key role in determining their properties.[4] For example, it has been found that a high amine content in the ligand shell could increase the PLQY, due to the enhanced oleylammonium bromide ($NC(X)_2$) binding motif of the carboxylic acid (**Figure 3c**).[100] The ligands exchange mechanism of the $NC(X)_2$ is shown in the following Equation 1:

$$NC(X)_2 + (X')^+(X')^- = NC(X')_2 + (X)^+(X)^- \quad (1)$$

Oleylamine is first involved in the acid/base equilibrium with hydrogen bromide and binds to the surface as $NC(X)_2$. Then, it deprotonates OAC and forms oleylammonium oleate. In this reaction, the oleylamine binds X-type ligands (donating one electron) by coordinating to the surface cations. However, it is also possible to bind L-type ligands, which could donate two electrons. Zhang's group used amino and carboxylic functional groups as passivating ligands, achieving well-passivated PNCs.[101] They explained that the protonation reaction between -NH_2 and -COOH was essential for successful passivation (**Figure 3d**). Except amino and carboxylate groups, phosphonate functional unit, when introduced into the ligands, can also affect the PNC stability. Wang *et al.* replaced the conventional OA with an alkyl phosphonic acid (TMPPA) to grow the $CsPbI_3$ NCs, demonstrating that the optical stability was significantly improved.[102] In addition to the above-mentioned functional groups, other inorganic capping ligands, such as $PbSO_4$-oleate[103] sulfobetaine, phosphocholine and γ-aminoacid sulfobetaine, could also affect the PNC stability and PLQY.[104] The chain length, chain type, amount, and ratio of the ligands can effectively influence the morphologies of the PNCs. By employing different lengths of carboxylic acids and amines (from 18 carbons down to 2 carbons) as capping ligands, various thicknesses and shapes of $CsPbBr_3$ NCs were obtained (see **Figure 3e**).[53] Li's group revealed that branched alkyl chain amino capping ligands can control the PNCs size and stability, due to the strong steric hindrance hampering the dissolution of the formed PNCs.[105] Moreover, by using large amount of OLA, the PNC surface became more protected in all directions and formed nanocubes, while otherwise nanorods were formed (**Figure 3f**).[106] Wang's group found that by tuning the ligand participating in the reaction such

as changing the amount of OAC and oleylamine, different shapes of PNCs can be achieved, such as nanowires or nanosheets (**Figure 3g**).[107] Since halide atoms can easily escape from the PNCs, resulting in their poor stability, surface passivation can be used to form more stable halide-hydrogen bonds on the surface, which could inhibit the capture of the excited electrons.[99] In addition, surface passivation affects the morphology of PNCs during the synthetic process. Hence, while surface ligands play a key role in controlling the reaction and formation of the PNCs, surface passivation is extensively beneficial to the stability and the optoelectronic properties, as will be discussed in the following subsections.

3.2 Stability

Most of PNCs exhibit poor stability, due to the considerable ionicity of the Pb-halide bonds and the rather dynamic nature of the ligand binding. Several key factors, namely halide composition, moisture, temperature, and UV light,[108] significantly impact on the stability of PNCs, consequently influencing the design of an optimum synthetic route to obtain highly stable PNCs. It has been found that bromide-based PNCs (*e.g.* $MAPbBr_3$) are more stable than the iodide-based ones (*e.g.* $MAPbI_3$), mainly due to the difference between the ionic radius of anions I^- and Br^-.[10] In the 6-fold coordination, the radii are 2.2 Å and 1.96 Å for I^- and Br^-, respectively, which create a distortion of the octahedrons.[10] It is worth noting that, despite $MABr_3$ showing higher stability than $MAPbI_3$ due to higher symmetry, the best performance for photovoltaic applications is achieved with $MAPbI_3$. An optimum combination of such structures was proposed by tuning the stoichiometry of $MAPbI_{3-x}Br_x$ (x = 0–1). By varying the humidity, the most stable PNCs were obtained when bromide constituted the 20 % of total halide content (*e.g.* x=0.2), due to the higher symmetry achieved in this nanostructure.[10]

Later on, Kovalenko's group reported an alternative synthesis route that was not employing a polar solvent to initiate the formation of PNCs.[109] The stability reported for such a colloidal solution exceeded three months. Nevertheless, the as-prepared PNCs suffered from severe

instability in presence of moisture. They could not be easily isolated in a purified state while using bad solvent without decomposing.

It is also known that the crystallization of PNCs is another key parameter in relation to stability.[110] Yuan's group reported that smaller clusters of cuboid $MAPbI_3$ NCs are more stable than the larger ones.[111] This might be correlated to better crystallinity of the smaller clusters. Recent studies involving 1D perovskite nanowires also support this argument.[112] Another way to drastically improve colloidal $CsPbX_3$ NCs stability is the exposition to X-Ray. In fact, X-Rays enhance the intermolecular C=C bonding of the organic ligands that coat the PNCs surface.[113]

UV light exposure is a known root of degradation for hybrid halide perovskites, though less investigated than other sources (*e.g.* moisture). UV light affects the structure and optical properties of perovskites, yet the exact degradation mechanism is still not fully clarified. Gao *et al.* reported on the influence of UV light illumination on the structural and PL properties of $CsPbBr_3$ PNCs, and they attributed the PL degradation to the photo-oxidation of lead atoms on the PNCs surface.[114,115] Ouafi *et al*. demonstrated that, by incorporating more than 20% of Br in $CH_3NH_3Pb(I_{1-x}Br_x)_3$ films, it is possible to clearly improve the stability of the films towards UV-light degradation because of the structural transition from the tetragonal phase to the more stable cubic crystal structure.[116]

The UV light-induced degradation is especially challenging when thinking of PDs for spectral regions including UV-C (280-200 nm) and even far UV (200-10 nm).[117] However, UV-induced damage specifically related to PDs is not very well documented in the literature. On the other hand, studies on the UV-degradation of PSCs, and possible solution to enhance their lifespan, are widely available.[118,119] It is worth highlighting that, both for PSCs and PDs, further studies to clarify the effects of reversible and irreversible UV-induced degradation mechanisms under realistic experimental conditions are urgently needed.[120,121] Currently, there is no intensity specification regarding UV light for wavelengths shorter than 400nm on the

standardized test conditions for solar simulator.[119] Furthermore, the widely adopted degradation tests under continuous light do not consider the light-dark cycles with temperature variations, as in real conditions. Finally, in the case of PDs, on/off measurements are often reported without clear indication of the measurement frequency. Thus, a fair comparison between different published results is not always easy.

As mentioned above, the characterization of the photophysical properties of PNCs, such as the change of absolute PL intensity or PLQY, and the lifetime of TRPL decay as a function of storage time, is an effective way to assess PNCs' stability. It is well known that $CsPbI_3$ PNCs suffer from a straightforward phase transition from cubic to orthorhombic phase.[122] Wang's group was able to stabilize cubic $CsPbI_3$ PNCs (see **Figure 3h(i, ii)**) by replacing the traditional OA ligand with an alkyl phosphinic acid.[102] Upon the replacement of the ligands, the as-synthesized PNCs remained photoluminescent for over 20 days, while the NCs with conventional OA exhibited nearly no emission after 3 days. A novel nanocrystal architecture, $CsPbX_3$/ZnS heterodimer, was reported by Chen's group via a facile solution-phase process.[123] When comparing the PL stabilities for pristine $CsPbBr_{3-x}I_x$ and $CsPbBr_{3-x}I_x$/ZnS heterodimers (see **Figure 3h(iii, iv)**), it was found that the ZnS dimers could effectively protect NCs up to approximately 12 days in air, while pristine $CsPbBr_{3-x}I_x$ NCs turned unstable and showed blue-shifted PL within 1 day. Shen's group employed trioctylphosphine (TOP) as a new type of ligand to synthesize high PLQY (nearly 100 %) $CsPbI_3$ QDs, retaining ~85 % of their initial QY after 1-month storage. In comparison, when a conventional oleylammine ligand was used, QDs showed a persistently decreased QY from the initial 86 % to 60 % after 30 days of storage (see **Figure 3i(i)**). The authors suggested that the reason for the stability enhancement can be attributed to the better chemical stability in TOP-QDs, which originates from the improved crystalline quality induced by the TOP ligands.[124]

TRPL studies have been conducted to assess the stability of Pb-free PNCs as well. Marcus *et al.* followed the PL evolution of a batch of $CsSnBr_3$ PNCs after one-week storage in an argon-

filled glovebox, showing an accelerated faster PL decay component from original 0.7 ns in fresh sample to 0.24 ns in aged sample while there was no obvious change for the slow decay component (see **Figure 3i(ii)**). Such a component results from the nonradiative decay at deep acceptor states, which have been developed slowly after synthesis.[125]. However, the decay constant for the slower component remained nearly the same in both aged and fresh samples. Ligand-free $Cs_3Bi_2Br_9$ PNCs reported by Han's group show very high stability with even improved PL decay lifetime after 22 days of air storage (see **Figure 3i(iii)**). This provides a promising alternative system for air-stable lead-free PNCs.[69] Recently, further studies demonstrate the role of doping,[30] surface passivation,[95] and crosslinking[126] in significantly enhancing the PNCs stability. Nevertheless, currently there are no examples in the literature where these techniques are combined in the same type of PNCs. We foresee that this could be a promising route to improve the stability of PNCs even further.

3.3 Tunable optical spectrum

Colloidal lead-based PNCs containing organic groups, *i.e.* $MAPbX_3$ or $FAPbX_3$, were synthesized for the first time by Galian *et al.* [41]. They reported stable $MAPbBr_3$ PNCs emitting green light, by using a medium alkyl chain of ammonium bromide as a stabilizer in the suspension. Later Yuping's group[36] developed the LARP method (see Section 2.1.1) to obtain $MAPbX_3$ QDs, by changing the amount of halide elements (X = Cl, Br, I). Their $MAPbX_3$ QDs exhibited very broad and tunable absorption with emission bands covering the whole visible spectral range till low NIR spectral limit (the emission onset is up to 780 nm). They also successfully controlled the emission bandwidth in a very narrow range with a FWHM of 20 – 50 nm, while showing relatively high PLQYs ranging from 50 % to 70 %. Later on, Rogach's group[49] continued to develop the LARP technique by varying the antisolvent's temperature to produce tunable optical spectra (**Figure 1c**) of $MAPbBr_3$ QDs with narrow emission line-widths of 28 – 36 nm. The possibility of bandgap tuning was realized for the first time for $MAPbX_3$ PNCs with X = Br. These PNCs displayed also a very high PLQY of 93 %, and good

crystallinity due to high precipitation temperature. In addition, Zhang *et al.* were able to synthesize uniform $MAPbX_3$ PNCs with tunable nanocrystal size (within 2.5 – 100 nm) and emission (452 – 524 nm) (see **Figure 4a**), and various PLQYs (*e.g.* 15 – 55 %), by controlling the concentration of capping ligands in the reactant precursor. To further extend the emission spectral range into the infrared region (wavelengths longer than 800 nm), $FAPbI_3$ PNCs with slightly lower bandgap than $MAPbI_3$, have been synthesized, demonstrating better temperature and moisture stability.[127,128] To overcome the recurrent instability of PNCs containing organic cations (*e.g.* MA^+ or FA^+) in ambient conditions, fully inorganic lead-based PNCs, such as $CsPbX_3$, have been widely investigated. The bandgaps and emission bands of $CsPbX_3$ NCs can be easily tuned over the entire visible spectral range by employing the similar strategy of varying the halide (X = Cl, Br, I) compositional ratio, as conducted for the hybrid organic-inorganic PNCs (*e.g.* $MAPbX_3$ or $FAPbX_3$) mentioned before. Protesescu's group[35] estimated the Bohr exciton diameters to be 5 nm, 7 nm, and 12 nm for $CsPbCl_3$, $CsPbBr_3$, and $CsPbI_3$, respectively. It is well known that if the edge length of a nanocrystal is smaller than the Bohr exciton diameter, it is possible to tune the emission wavelength and the corresponding PLQY upon quantum size effect. Accordingly, they obtained tunable emission spectral range with a FWHM of 12 – 42 nm and PLQYs of 50 – 90 % for $CsPbX_3$ QDs (**Figure 4b**).[129] Furthermore, some other low-dimensional $CsPbX_3$ NCs, *i.e.* 1D nanowires and nanorods (see **Figure 4c(i, ii)**) and 2D nanoplatelets and nanosheets (see Figure 4c(iii, iv)), have also been successfully produced via solution-phase synthesis, by controlling the amount of capping ligands such as oleic acid and oleylamine.[44,130,131] Bekenstein *et al.* reported highly emissive $CsPbBr_3$ nanoplatelets consisting of various numbers of unit cells, demonstrating the thickness dependent optical properties.[132] Due to quantum confinement effects, the $CsPbBr_3$ nanoplatelets exhibited a clear trend of blue-shift when decreasing the thickness (see **Figure 4d**).

As discussed in Section 2.3, it is paramount to replace Pb in PNCs with alternative non-toxic metal cations, ideally light metals. The absorption and emission wavelengths of PNCs based on Sn, $CsSnX_3$, were tuned from the visible region to the NIR spectral range by varying the compositional ratio of halides (X = Cl, Br, I). Particularly, $CsSnI_3$ NCs absorb a very broad spectral range with absorption onset up to 900 nm, which is much wider than that of the Pb-based counterpart.[12] Consequently, $CsSnI_3$ PNCs could be favorable for broad light harvesting.[125,133] However, $CsSnI_3$ PNCs show extremely low PLQY, mainly due to the high defect density on the surface caused by the undesired oxidization of Sn^{2+} to Sn^{4+}.[134] The Cs_2SnI_6 PNCs, with a proposed A_2BX_6 crystalline structure (see Figure 5c(i))[125] in different morphologies (see **Figure 5a** and **5b**), [135] present a slight blue-shift of the optical spectra for the as-prepared crystals with the increase of reaction time. PNCs based on trivalent metal cations in the B-sites of $A_3B_2X_9$ structure (see **Figure 5c(ii)**) were first theoretically designed [136] and then recently synthesized [69]. $Cs_3Bi_2X_9$ PNCs (see Figure 5d) have an emission band in the range between 400 nm and 560 nm. More surprisingly, $Cs_3Bi_2Br_9$ PNCs display high stability without obvious drop in the PLQY, even if stored in air conditions for over 30 days.[137] A post-synthetic anion exchange treatment on the as-synthesized PNCs allows the tuning of halide compositions, leading to a tunable emission wavelength ranging from 390 to 570 nm (see **Figure 5e**). From the fully inorganic halide double PNCs with a proposed structure $A_2BB'X_6$ (see **Figure 5c(iii)**),[18] only Cs_2AgBiX_6,[18,138,139] Cs_2AgInX_6,[140] and $Cs_4CuSbCl_{12}$[141] have been successfully synthesized to date. However, most of the known double PNCs have a large bandgap of over 2 eV, and thus are not suitable for light harvesting. Therefore, the bandgap engineering is urgently required to fine-tune the optimum level of bandgap for double PNCs, as will be discussed in subsection 3.5.

3.4 Time-resolved studies

The time-resolved spectroscopy studies go beyond the optical properties in ground state (achievable by steady-state spectroscopy), and can effectively provide comprehensive

understanding of the fundamental photophysical and photochemical processes, such as the excited-state lifetimes and charge carrier transfer kinetics. This information is crucial for further applicability of PNCs in optoelectronic devices.[142–144] There are mainly two time-resolved techniques, *i.e.* time-resolved photoluminescence (TRPL), or so-called transient emission spectroscopy (TES), and transient absorption spectroscopy (TAS). TRPL characterization is obtained by exciting a sample with a pulsed laser, and by monitoring the PL intensity as a function of time. TAS is also known as a pump-probe spectroscopy that allows revealing the ultrafast (fs to ps) or fast (ns to μs) dynamics of the photoinduced species in different energy states, *i.e.* excitons, free charge carriers (electron and hole) and polarons. The monitored dynamics are generally determined by the characteristics of samples, including composition, crystallinity, morphology, particle size/shape, and surface passivation, particularly for PNCs in liquid or solid phase. We have reviewed the tunable optical spectra of PNCs with various compositional halides (X = Cl, Br, I) in the previous sections, which also affect the exciton dynamics of PNCs in the time-resolved characterization. Both Kovalenko's group[35] and Dong's group[145] reported that the radiative lifetimes of $CsPbX_3$ PNCs vary in the range of 1 – 29 ns with accelerated decays from I-based towards Cl-based PNCs (see **Figure 6a** and **6b**), resulting in improved stability but decreased performance. The presence of capping ligands with various chain lengths effectively influence the exciton dynamics of PNCs. $Cs_3Bi_2X_9$ PNCs, synthesized with and without OA ligand's capping function, exhibited distinguishable charge-carrier kinetics. Based on the bi-exponential fitting of the ultrafast PL decays (see **Figure 6c**), a long-lived component (200-300 ps) with increased contribution in OA-capped PNCs, and a fast component (< 20 ps) with corresponding decreased contribution compared to ligand-free PNCs, were found.[69] TAS measurements on the same PNCs showed the so-called decay-associated spectra (DAS) containing three components as depicted in **Figure 6d**. An ultrafast 2 ps component was observed, mainly attributed to a combination of Auger recombination and charge transfer from the excited state to trap states. Finally, the same co-authors formulated an

overall scheme that thoroughly clarifies the excited state dynamics as a function of capping ligands (**Figure 6e**), including fast trapping transfer (2-20 ps), Auger recombination, intrinsic radiative (300 ps), and the decay of the long-lived trapping state (> 3 ns), which enhance the PNCs PLQY.[69] The influence of the capping ligand length on the exciton dynamics was investigated by Zhang *et al.* who employed a short octylammonium bromide (OABr) and a long octadecylammonium bromide (ODABr) capping ligands in $MAPbBr_3$ PNCs.[146] The TA (see **Figure 6f**) and 3D TRPL results (see **Figure 6g**) indicate longer exciton lifetime of PNCs with OABr, attributed to a lower density of trap states by shortening OABr capping distance. This enhanced PLQY was correlated to the better solubility of OABr in the precursor during synthesis and consequently better surface passivation compared to the ODABr case (see a scheme comparison in **Figure 6h**).

The exciton dynamics of PNCs are strongly related to several other dominant parameters as well, such as reaction time and precipitation temperature. Kamat's group conducted ultrafast TAS measurements for the as-synthesized $CsPbBr_{3-x}I_x$ PNCs to clarify the influence of iodide amount on the exciton dynamics (see **Figure 6i** and **6j**).[61] The TA spectra (a) of $CsPbBr_3$ nanocrystals film in **Figure 6i** show strong ground-state bleaching (GSB) at 517 nm, corresponding to the band edge of $CsPbBr_3$. Along with the increase of iodide amount (spectra (b)-(f)) in the film, the main GSB red-shifts, consistently with the trend in steady-state absorbance. The TA decays of the PNC films in **Figure 6j** show that the charge recombination kinetics at the bleach maximum tend to be extremely fast at the initial stages of halide exchange (decays a, b). However, with the increasing of the exchange time, the bleach demonstrates slower recombination (decays c-f). This observation clearly proves that small amounts of exchanged iodide induce large amounts of non-radiative recombination for PNCs. Rogach's group investigated the dependence of exciton dynamics on the precipitation temperature in $MAPbBr_3$ PNCs.[49] Their work indicates that radiative lifetimes tend to decrease slightly as the emission shifts to longer wavelengths, while non-radiative lifetimes increase with the increase

of precipitation temperature. The highest PLQY of PNCs up to 93 %, and the longest non-radiative lifetime was achieved when the highest precipitation temperature (60 °C) was applied for the reaction. Based on their TEM studies, the high PLQY was assigned to high crystallinity induced by the high precipitation temperature.

The material band structure can also severely influence the charge carrier dynamics in PNCs. A so-called direct-indirect nature of bandgap in conventional bulk perovskite films (*e.g.* $MAPbI_3$) has been recently reported based on both theoretical calculations and experimental results.[147,148] This describes that the CBM of perovskites is slightly shifted in *k*-space compared to the VBM, thus making the bandgap indirect.[149,150] Zhang *et al.* observed a dual-spectral feature in the PL spectrum of $Cs_3Bi_2I_9$ NCs, assigned to the direct and indirect transitions during excitonic recombination (see **Figure 6k**).[151] They proposed a competitive recombination process between direction and indirection transitions. It is worth noting that the low PLQY (< 0.1 %) of $Cs_3Bi_2I_9$ NCs could be attributed to the presence of nonradiative recombination pathways, *i.e.* native defects, promoted by the indirect bandgap.[152] In the time-resolved spectroscopy studies, an indirect transition normally results in a much longer lifetime (several to hundreds of nanoseconds) than in a direct transition (tens of picoseconds to few nanoseconds).[147,153] Therefore, it is crucial to probe the excitonic recombination process with TRPL or TAS in proper time-scales.

In **Table 2**, we summarize the results from recent TRPL studies for various perovskite nanocrystals by correlating the PLQYs with the average PL decay lifetime (τ_{avg}), the radiative recombination lifetime (τ_r) and the non-radiative recombination lifetime (τ_{nr}). It can be noted that bromide-based hybrid PNCs (*e.g.* $MAPbBr_3$ or $FAPbBr_3$) generally exhibit relatively high PLQY compared to chloride- or iodide-based PNCs. This can be attributed to longer non-radiative recombination lifetimes obtained for bromide-based PNCs. Bromide anions are expected to well passivate the surface state, thus realizing a condition of high defect tolerance, which could be a useful feature for highly emissive layer in LEDs or displays. Recently, Liu *et*

al. have shown an outstanding PLQY (99%) for iodide-based perovskite nanosheets synthesized via a novel method called two-step hot injection. By fine-tuning key parameters, such as ligand concentration and injection temperature, $MAPbI_3$ nanosheets exhibited very long average lifetime (within 593 ns) in TRPL measurements, indicating that nearly defect-free iodide-based PNCs can be also obtained via effective surface passivation and dimensionality tuning.[154] It is also interesting to observe that with mixed organic cations (*e.g.* $FA_xMA_{1-x}PbI_3$) the PNCs show extremely long lifetimes for both radiative and non-radiative recombination, potentially allowing highly efficient charge transfer from excited state to charge acceptors (*i.e.* electron and hole transfer materials) if PNCs are used in solar cells.[155] In fully inorganic lead PNCs such as $CsPbX_3$, the PLQY dramatically fluctuates in a wide range closely dependent on the halide composition. A very high PLQY of nearly 100 % has been achieved by $CsPbI_3$ nanocrystals while showing high capacity of light harvesting, providing promise for light emission and photovoltaic applications.[124] Until now, most Pb-free perovskite nanocrystals present relatively low PLQY due to fast charge carrier recombination process, likely in relation to the above mentioned direct-indirect nature of bandgap. However, there are some exceptional case like Cs_2SnCl_6:Bi that shows quite high PLQY (*e.g.* ~80 %) with long-lived PL decay lifetime (*e.g.* τ_{avg} = 343 ns). When small amount of bismuth were incorporated into Cs_2SnCl_6 matrix at the Sn site, it forms the so called Bi_{Sn} + V_{Cl} defect complex with strong blue emission.[156] This method provides an alternative pathway to explore novel lead-free PNCs emitters.

3.5 Bandgap engineering

As an intrinsic property of semiconductor nanocrystals, the bandgap is always the key factor to for designing optoelectronic devices, as it strongly relates to the PNCs optoelectronic properties and to the performance of corresponding devices. For instance, high light harvesting of PNCs needed for solar cells is paramount, giving rise to high photocurrent due to strong light absorption. Thus, low-bandgap PNCs, *i.e.* ideally less than 1.5 eV, need to be designed and

synthesized, with absorption/emission onset at > 800 nm. Other applications of PNCs, such as LEDs and PDs, benefit from broad visible spectral region (400–700 nm). Hence, the bandgap of PNCs should be tuned in the range 1.7–3.0 eV to meet this requirement. Accordingly, various approaches of bandgap engineering for PNCs have been extensively investigated by the research community. Kovalenko's group utilized the concept of quantum-size effects to tune the size of $CsPbBr_3$ PNCs compared to its estimated Bohr exciton radius (*e.g.* 7 nm), as shown in **Figure 7a**.[35] By using a calculation method called effective mass approximation (EMA), they estimated a theoretical bandgap curve as a function of the nanoparticle diameter, in good agreement with their experimental results for the actual bandgap values shown in **Figure 7b**. It can be clearly observed that the bandgap of $CsPbBr_3$ PNCs increases with the decrease of nanocrystal size, as shown by the blue-shift in the absorption and emission spectra. Both Ravi's group[96] and Manna's group[57] tuned the bandgap of $CsPbX_3$ PNCs by varying the compositional halides (X = Cl, Br, I).[157] The VBM and CBM for $CsPbX_3$ PNCs were determined by electrochemical methods (cyclic voltammetry). As shown in **Figure 7c**, the VBM displayed a significant shift of 0.80 eV from -6.24 eV to -5.44 eV, whereas the CBM presented a weaker shift of 0.19 eV from -3.26 eV to -3.45 eV, along with the successful tuning of nanocrystal composition from $CsPbCl_3$ to $CsPbI_3$, through $CsPbBr_3$ and mixed halides $CsPb(Cl/Br)_3$ and $CsPb(Br/I)_3$. Hence, they concluded that, even if the halides contributed more to the VBM than to the CBM, their contribution to the CBM was also not negligible. By controlling the molar ratio between the added halide or exchanged halide and the Br amount in the starting PNCs, Manna *et al.* realized a precise bandgap tuning for $CsPbX_3$ PNCs, as shown in **Figure 7d**.[57] Furthermore, for 2D nanoplatelets or nanosheets, the thickness of PNCs, and thus their bandgaps, could be effectively tuned by readily changing the reaction conditions (such as the precipitation temperature), while keeping the other experimental conditions constant. In Dong *et al.*'s report,[145] the formation of thicker $CsPbBr_3$ nanosheets appears to be favored by the decrease of the reaction temperature and the lowering of the bandgap (see **Figure**

7e). For example, by carrying out reactions at 150 ℃ and 60 ℃, $CsPbBr_3$ nanosheets were achieved, whose thicknesses were ~2 nm and ~4 nm (corresponding to 2 and 4 monolayers, respectively) according to AFM studies. TEM studies confirmed the 2D planar geometry of those ultrathin $CsPbBr_3$ nanosheets (see **Figure 7f** and **7g**). Alex *et al.* summarized a scheme (see **Figure 7h** and **7i**) to exhibit the dependence of energy transfer mechanism on the number of monolayers in organic PNCs.[158] This mechanism could be employed to funnel energy from nanoplatelets or nanosheets with wide bandgaps to those with narrower ones improving the PLQY in the meanwhile. Such cascaded energy transfer processes have been utilized to enhance the emission of low bandgap regions in structures consisting of layer-by-layer assembled traditional semiconductor QDs.[159] It is worth noting that additional factors, such as structure phase and lattice parameter, can influence the bandgap even for the same type of PNC with identical composition.[56] For instance, when considering the cubic and tetragonal phases for $MAPbBr_3$ and $MAPbI_3$ PNCs, their bandgaps are 1.93 and 1.96 eV for $MAPbBr_3$, and 1.54 and 1.58 eV for $MAPbI_3$, respectively.

4. Applications

4.1 Light emitting diodes (LEDs)

The unique blend of emission characteristics of halide PNCs in the visible–NIR spectral region, namely the narrow emission bandwidths, high PLQY, broadly tunable color range, and an impressively wide gamut of highly saturated colors (**Figure 8a**), makes them attractive and promising light emitters for LED applications. Theoretically, there are two major strategies for assembling a color-converting emitter into a lighting device, denoted as “on-chip” and “remote phosphor” configurations.[29] In the “on-chip” configuration, the PNC emitter is formed directly onto a base LED, resulting in a substantial heat transfer to the PNCs through a very high local flux of UV or blue light.[4] In the “remote phosphor” configuration, the PNC emitter is located remotely from the LED light source, *i.e.* a PNC film can be deposited on the surface area of the light fixture.[29] In both configurations, the operation temperature should be below 100 ℃. A

typical structure of a three-color LED pixel with a thin layer of PNCs as the emitter is shown in **Figure 8b**.[4] Basically, the radiative recombination of electrons and holes injected from corresponding electrodes into a thin PNC layer, *i.e.* the electroluminescence (EL), is more relevant than PL to evaluate the operation of LEDs in display applications (see **Figure 8c**).[78] The EL efficiency of LEDs is correlated to the charge carrier dynamics according to previous reports.[46,94] In order to obtain high EL efficiency, effective charge carrier (electron and hole) injection at the interface between PNCs and charge selective layers (ETL and HTL) is paramount, which is directly related to the lifetime of the TRPL decays. For instance, swift electron or hole injection results in accelerated TRPL decays with short lifetime (hundreds of picoseconds to several nanoseconds), while excited state decays for PNCs have long lifetimes (hundreds of nanoseconds). Furthermore, the charge carrier transport within PNCs should be also prompt and efficient to realize high emission mainly through radiative recombination pathways, since the nonradiative recombination processes are known to quench the photoluminescence.[78] Both charge injection and charge transport processes dominate the overall internal quantum efficiency (IQE) in PNCs-based LEDs, in straightforward relation with their EL efficiency. Therefore, a known correlation between LED efficiency and the corresponding photophysical characteristics is crucial to acquire hints for further development of high performance LED devices.

However, the low EL efficiency is still a critical drawback when aiming to efficient PNC-based LEDs.[78] Park's group reported a bilayer PNC structure leading to a current efficiency (CE) of 42.9 cd A^{-1}, which represents a two orders of magnitude enhancement compared to the CE of LEDs based on a conventional bulk crystal perovskite structure.[6] To further boost the EL yield, Tan's group fabricated a highly efficient $CsPbX_3$ LED by using a new trimethylaluminium (TMA) vapor-based crosslinking method (**Figure 8d**).[160] Due to the insoluble crosslinked PNC film, the formation of subsequent charge-injection layers with no orthogonal solvents was realized. The high-quality crosslinked $CsPbX_3$ NC film reached the needed quantum

confinement of the injected charge carriers. This effect promoted the electron-hole radiative recombination, thus leading to promising EQEs of 5.7 % for red emission, and 0.19 % for green emission. Some other studies on the interfacial engineering have also shown potential to improve the charge injection at the interface of PNCs film. Zhang's Group produced high-performance PNC LEDs with improved brightness and narrow green emission (*e.g.* FWHM = 18 nm), involving a novel thin film of perfluorinated ionomer (PFI) sandwiched between the perovskite emitter and the HTL. In this system, the hole injection was promoted upon the insertion of the PFI thin film that at the same time prevented the PNC emitters from charging.[161]

Several other strategies to target high-efficiency PNC-based LEDs have been developed. For instance, a so-called quantum well structure has been involved to effectively confine the electrons and holes, resulting in the enhancement of the radiative recombination.[16] By employing multi-quantum wells, Wang's group successfully fabricated a red PNC LED with very high EQE of 11.7 %, which has been accounted as the latest record for PNCs-based LEDs. Despite the development of efficient monochromatic PNC LEDs, there is a recent trend to achieve white-light EL from PNC LEDs with complete colour tunability throughout the visible spectral region. To date, PNC-based white-light emission has been achieved through photoexcitation in layered perovskites with a so-called self-trapped emissive states[162] and through a mixture of colorful PNCs localized in a polymer matrix (**Figure 8e**).[163] Other strategies, including the construction of multi-ion PNCs and light extraction skills, also demonstrated attractive ways to enhance device performance.[65,164] In addition to the design and engineering of various PNCs for LEDs, the fine tuning of the LEDs device structure also plays an important role when aim at performance enhancement of LEDs. Friend *et al.* successfully introduced perovskite technology into the application of LEDs for the first time within the structure 'ITO/PEDOT:PSS/perovskite/poly(9,9-dioctylfluorene)(F8)/Ca/Ag' via a solution process, leading to bright green LEDs with an EQE of 0.1 %.[25] Later on, promoted

by the skyrocketing evolution of PSCs, most of 3D-perovskite-based LEDs were simply developed with similar device architectures as the corresponding photovoltaic devices.[165–167] For PNCs based LEDs, their dimensionality in the forms of QDs, NCs, NWs, or nanoplatelets, have shown variable impacts on the optimization of the device structure. **Figure 8f** shows the typical device structure of multilayered LEDs based on $CsPbX_3$ QDs, reported by Zeng *et al.*[5] They first demonstrated the multicolored LEDs based on fully inorganic perovskite QDs, showing an EQE of 0.12 % for green LEDs and sharp emitted lights for all colors. Vertically oriented perovskite nanorods (NRs) or nanowires (NWs) have also been applied in LEDs, as the vertical geometry could enlarge active surface area and inspire an enhanced charge carrier transport. Yang *et al.* first assembled $MAPbBr_3$ NRs- based LEDs with a representative device structure shown in **Figure 8g**. Their results show that the turn-on voltage for EL at room temperature was about 3.5 V of DC bias, which represented a 0.2 V improvement compared to the bulk film corresponding device.[168] Similarly, perovskite nanosheets or nanoplatelets could also provide promising performance in LEDs due to their high crystallinity and PLQY. Ling *et al.* integrated hybrid perovskite nanoplatelets into the bipolar PVK:PBD matrix to improve the film morphology and charge transport properties.[169] The strategy of polymer-matrix-assisted light emission holds great potential for the assembling of white-light PNCs based LEDs via the embedding of perovskite nanostructures with variable emitted colors.

The performance of recent PNC-based LEDs is summarized in **Table 3**. It is worth noting that Pb-based PNCs still dominate the LED applications due to their excellent EL properties compared to the Pb-free PNCs. However, there are still two main issues hindering the development of efficient PNC-based LEDs which need to be solved: the enhancement of the (1) internal quantum efficiency (IQE) and of the (2) light out-coupling efficiency. To increase (1), there is an urgent request for thorough interfacial engineering towards efficient charge dissociation and transfer. The fine-tuning of the band levels between PNC layer and the charge transfer layers could also be a key point for improving the IQE. To enhance (2), optical

engineering could be an effective way to extract the trapped waveguide and surface plasmon modes induced by the high refractive index of perovskite nanomaterials.[46]

In addition to the challenge of improving the performance of PNC LEDs, the poor stability originated from the perovskite itself,[170,171] the ion migration,[172] and the metal electrode diffusion[173] are still the main concerns for future commercialization. Several strategies have been recently proposed to address the stability issues. One idea is to employ all-inorganic perovskite materials to provide a potential long-term solution,[46] while alternative approaches are based on the introduction of large organic ammonium cations to form a Ruddlesden-Popper layered perovskite, which could effectively hinder ion migration and thus improve PNCs stability.[16]

4.2 Solar cells

In the last decade, light absorbers based on halide perovskites have significantly progressed in high-performance solar cells with best PCE up to 23.7%[174]. Although there are countless research articles on the development of photovoltaics based on perovskite bulk films, on the other hand only a few reports have been targeting the application of PNCs in solar cells. In theory, a highly-efficient solar cell can only be realized through the precise control of three dominant factors, namely light harvesting, charge separation, and charge transport. As discussed in Section 3, the optical spectrum of PNCs can be fine-tuned, which is beneficial to obtain high absorption in a broad wavelength range. However, the preparation of thin films with high-quality (*i.e.*, smooth, compact, and with less defects) and good connectivity for efficient charge separation and charge transport using nanocrystals is still challenging. In particular, the bulky organic ligands often used in the synthesis of PNCs will impede the connectivity of the nanocrystals with charge acceptors (*e.g.* ETL and HTL), and thus hinder the charge transport process, with detrimental effects on the overall internal quantum efficiency (IQE). Therefore, proper post-treatment steps, such as ligands exchange or removal of ligands, have been considered to improve film quality and stability. A breakthrough occurred when Swarnkar *et*

al. reported 10.77 % efficient ambient air stable PNCs device based on cubic $CsPbI_3$ (or α-$CsPbI_3$).[175] They found that the unstable cubic phase of $CsPbI_3$ is air stable in the nanocrystalline form. Moreover, they applied methyl acetate to remove the ligands as post-treatment method. The use of methyl acetate as the antisolvent played a key role in the purification stage, which removed excess unreacted precursors limiting the aggregation. Upon the extraction process, both α-$CsPbI_3$ QDs and QD films were stable for several months under ambient storage conditions.

Moreover, Zhang *et al.* have pointed out that lowering the dimensionality of PNCs from 3D to 2D or 1D could potentially solve the charge transport issues because lower dimensional nanocrystalline perovskites presented a slower recombination rate when compared to higher dimensional PNCs.[46] Grätzel's group reported the first example of perovskite nanowires (NWs) based solar cell.[176] They successfully realized the formation of $MAPbI_3$ NWs by coating the PbI_2 layer with a 2-propanol solution of MAI in the presence of a small volume of a polar solvent (DMF). The charge separation at the interface between perovskite and HTL was faster for 1D nanowires compared to 3D nanocubes, resulting in a champion solar cell achieving at most a PCE of 14.7 %. Nevertheless, solar cells based on perovskite NW still show lower PCEs compared to conventional devices based on bulk films, mainly due to two key reasons: 1) the charge transport could still be influenced by the presence of the template such as the axis of NWs; and 2) the contact between perovskite NWs and ETL or HTL needs to be still enhanced due to the uncontrollable orientation of NWs. Therefore, it is crucial to make more research efforts on the synthesis of vertical perovskite NWs without template and on the optimization of the contact between PNWs and charge acceptors. It is well known that hybrid organic-inorganic PNCs (*e.g.* $MAPbX_3$ and $FAPbX_3$) show lower stability compared to fully inorganic PNCs such as $CsPbX_3$, which is in turn a critical barrier towards commercialization. Thus, the $CsPbX_3$ PNCs have been successfully employed in solar cells. In addition to the stable cubic $CsPbI_3$ previously mentioned, a so-called A-site cation halide salt (AX) treatment has been reported to

effectively enhance the charge carrier transport.[177] Luther's group concluded that this AX treatment could tune the coupling between perovskite QDs, leading to the improved charge collection efficiency for the achievement of high PCE (13.43 %) in solar cells. Moreover, cubic $CsPbI_3$ could also be used as an interfacial layer to tailor the energy cascade level due to its high VBM and high moisture resistance. Liu's group combined a $CsPbI_2Br$ bottom cell with a $CsPbI_3$ QD top cell to obtain well-tuned energy levels, extending photoresponse and enhancing carrier mobility for a significant improvement in the PCE (*e.g.* 14.45 %).[178] There are also some other engineering strategies to continuously improve the performance of PNCs based solar cells mainly including incorporation of PQDs in organic bulk heterojunction blends,[179] mixing different dimensional PQDs,[180] use of polymer (PVP) as a stabilizing agent,[181] incorporation PQDs into graphene,[182] surface ligand management,[183,184] and the study of $CsPbI_3$ with novel hole conductors,[185] whose key performances have been summarized in Table 4.

4.3 Lasers

The use of perovskite materials as light-amplifying medium in laser applications has followed the rapid development seen in solar cell efficiencies. The first demonstrations of the potential in laser applications came in 2014, when Xing *et al.* reported the gain properties of bulk $CH_3NH_3PbI_3$ thin films, noting that amplified spontaneous emission (ASE) can also be seen in functional photovoltaic devices. ASE thresholds as low as 12 $\mu J/cm^2$ were recorded with 600 nm, 1 kHz, 150 fs pump pulses, and lasing inside a microcrystal formed in a drop cast film was observed.[186] Room-temperature, continuous wave operation was achieved in 2018 by Li *et al.* with a distributed feedback (DFB) laser design utilizing thermally nanoimprinted film of $CH_3NH_3PbI_3$.[187] The imprinting process significantly improved the crystalline quality and surface roughness of the perovskite material, and with an optimized feedback structure allowed power thresholds as low as 13 W/cm^2 in ambient conditions.[187] The improved crystalline quality decreased scattering from grain boundaries within the perovskite film, reducing the

amount of optical gain required for laser operation. An alternative way of reducing the effects of grain boundaries in laser applications is to use nanocrystalline materials, essentially making the grain boundaries much smaller than the wavelength of light. Utilizing PNCs instead of bulk crystals accomplishes this, in addition to providing both size-tunable and composition-tunable optical properties. This allows the use of the PNCs in lasers spanning the visible spectrum. The first PNC-based lasers were reported in 2015, when Yakunin *et al.*[188] and Wang *et al.*[189] both demonstrated lasing in whispering gallery mode (WGM) resonators coupled with inorganic $CsPbX_3$ nanocubes. A lasing threshold of 11 mJ/cm^2 was observed for a 50 μm diameter microcapillary infiltrated with $CsPbBr_3$ quantum dots.[189] The ASE thresholds from thin films were much lower than the lasing thresholds observed, with 22 $\mu J/cm^2$ for $CsPbBr_3$ reported by Wang *et al.* and 5 $\mu J/cm^2$ by Yakunin *et al.* For $CsPbCl_3$ PNCs the ASE threshold was found to be 11 $\mu J/cm^2$, and for $CsPbI_3$ PNCs 22 $\mu J/cm^2$, showing composition-tunable gain from 460 nm to 630 nm.[188] In all these experiments the PNCs were optically pumped using 400 nm, 1 kHz, 50-100 fs laser sources.

A significant improvement in the lasing thresholds was found in microcavities, where a thin layer of $CsPbX_3$ NCs is sandwiched between two highly reflective mirrors. In this configuration Wang *et al.*[190] reported lasing thresholds of 11 $\mu J/cm^2$, 19.0 $\mu J/cm^2$, and 25.5 $\mu J/cm^2$ for $CsPbBr_3$ (green, 510 nm emission), $CsPb(I/Br)_3$ (red, 595 nm emission), and, $CsPb(Br/Cl)_3$ (blue, 470 nm emission) devices, respectively (see **Figure 10a** and **10b**). The lowest lasing threshold reported for $CsPbBr_3$ NC-based microcavitites is 0.39 $\mu J/cm^2$ by Huang *et al.* (see **Figure 10c** and **10d**) who optimized both the gain material quality and matched the optical cavity resonance to the maximum gain wavelength by tuning the $CsPbBr_3$ layer thickness.[191] These low lasing thresholds were achieved with optical pumping using 50 – 100 fs pulses at 400 nm, with 1 kHz repetition frequency. Both groups also measured their microcavities using nanosecond pulsed laser excitation. The lasing thresholds were increased by roughly two orders of magnitude, from 11 $\mu J/cm^2$ to 900 $\mu J/cm^2$ for Ref.[190] and from 0.39 $\mu J/cm^2$ to 98 $\mu J/cm^2$ for

Ref.[191] compared to femtosecond optical pumping. The increase in the lasing threshold is attributed to the relatively short nonradiative Auger recombination lifetime, on the order of 100 ps [189], which reduces the effective optical gain. The increased pump intensities combined with the low thermal conductivity of the PNCs brings some concerns for device stability due to self-heating of the material. The lifetimes of the laser devices were significantly reduced when using nanosecond pumping.[191] Cooling of the microcavity down to 10 K increased the device lifetime, however the rate of degradation in output power was still approximately 500 times faster compared to the case of fs-laser pumping in ambient conditions.[190]

Patterning of the PNCs into microscale structures is essential for creating integrated laser devices. To this end, Lin *et al.* introduced a fluorinated polymer-based photolithography method, where the non-solubility of the $CsPbBr_3$ NCs in fluorinated solvents was used in lift-off patterning on arbitrary substrates. Microdisk lasers made with this technique showed lasing thresholds of 200 $\mu J/cm^2$, when excited by 450 nm, 7 ns pulsed laser source.[192] In contrast to the accurately patterned lasers, in random lasers the optical feedback comes from loops formed by random scattering.[192] Li *et al.* used PNCs anchored onto silica nanospheres to create luminescent PNC-SiO_2 composite films that show random lasing with thresholds down to 40 $\mu J/cm^2$ when optically pumped with 100 fs, 400 nm pulses.[193] Perovskite nanowires and nanoplatelets can act as standalone laser cavities when their sizes are increased above 100 nm in two dimensions. Light can be guided along a nanowire similar to optical fibers. Depending on the diameter of the wire, there can be either single or multiple transverse optical modes. The end facets of the nanowire will reflect part of the light back, forming the laser cavity with optical modes spaced inversely proportional to the length of the nanowire. With sufficient optical pumping both single and multimode lasing are possible inside the nanowire.[194–199] Inside a nanoplatelet, light can be trapped in whispering gallery modes, where photons circulate in a closed loop inside the platelet due to total internal reflection at the edges. Light propagating in these loops can be amplified when the platelets are optically pumped.[23,200,201]

4.4 Photodetectors

Perovskite, the wonder material for photovoltaics, has lately shown potential in photodetectors (PDs) because of its suitable bandgap, high sensitivity, ultrafast response speed to visible light, and high photovoltage.[202–205] Furthermore, solution processability and easy integration in both rigid and flexible substrates make perovskite materials attractive for PDs fabrication. For practical applications, PDs need to meet the so called '5H-s' requirement: high sensitivity, high signal-to-noise ratio, high spectral selectivity, high speed, and high stability.[206] Most materials suitable for solar cells are also suitable for PDs, since both technologies involve electrical charge generation by optical stimulus and charge collection.[46] An overview of the performances of key PNCs-based PD systems is summarized in **Table 5**.

The first study on perovskite-based PDs consisted of continuous films of tiny perovskite particles, leading to devices with ultrafast speed and good overall performances.[207–209]However, PNCs with low 2D or 1D morphologies perform better than thin films or bulk crystals due to the high excitonic binding energy and nanoscale quantum confinement.[204]

The compatibility of perovskite materials with both rigid and flexible substrates allowed Zeng *et al.* to report the first solution-processed PD based on 2D $CsPbBr_3$ nanosheets on flexible substrate, as illustrated in **Figure 10a**.[205] The device structure consists of ITO/$CsPbBr_3$ nanosheet/ITO and Au/$CsPbBr_3$ nanosheet/Au, with $CsPbBr_3$ nanosheets dispersed on patterned ITO or Au/PET substrates. The illumination of the photoactive area generates electron-hole pairs that are transported and collected at their respective electrodes (**Figure 10b**). These PDs showed high photosensitivity with on/off ratios higher than 10^3, and high stability with a fluctuation of less than 2.6% after 12 h irradiation with a 442 nm and 10 mW cm^{-2} laser. It is worth noting that these devices exhibited an outstanding flexibility. After bending them about 80º for 10 000 times, they still showed high on/off ratio, demonstrating excellent stability upon bending in ambient conditions (**Figure 10c**). The high stability can be ascribed to their all-inorganic composition, while the excellent flexibility can be attributed to their unique 2D

features such as the structural relaxation. It is also demonstrated that, after functionalization of $CsPbBr_3$ nanosheets with carbon nanotubes (CNTs),[210] the corresponding PDs still exhibited good flexibility and stability. In addition, their performance was significantly enhanced as compared to that of PDs with pristine $CsPbBr_3$ active layers. The best performance was obtained with the CsPbBr3 nanosheet/CNT composite with 6 % CNT volume ratio, with the EQE enhanced from 54 % to 74.88% and the responsivity increased from 0.64 to 31.1 A W^{-1} compared to the bare $CsPbBr_3$ nanosheet. The addition of CNT into perovskite nanosheets enhances the active layer conductivity, carrier extraction, and carrier transport, thus resulting in improved performance. However, when the CNT volume is increased above the optimal 6% ratio, the PD performance, typically the EQE, decreases due to the weak light absorption.

The 2D PNCs have also been adopted in vapor phase for PD applications through methylammonium iodide vapor carrier and PbI_2,[211] in addition to the above mentioned solution-processable approach. Although the synthesis route follows complicated steps, the PDs through vapor phase approach leads to better performance in comparison to the ones via solution-based approach due to the high-quality PNCs produced by the vapor reaction method. When 2D $MAPbI_3$ PNCs were sandwiched between highly conductive graphene layers in PDs (device structure: graphene/2D $MAPbI_3$ NCs/graphene), a high photoresponsivity of 950 A W^{-1}, an on/off ratio $\sim 10^6$ and a photoconductive gain of around 2200 were achieved.[211] Furthermore, this work also demonstrated that an addition of ultrathin boron nitride (BN) layer acted as an efficient protection layer at the top and bottom of PNCs. The BN-protected PD showed no damage and no considerable degradation after 210 days, while the unprotected PD displayed severe damage already after 37 days (**Figure 10d**). An alternative approach to enhancing the stability under continuous irradiation is proposed by Li *et al.*,[210] who built compact and smooth carrier channels for optoelectronic devices using the concept of self-healing at room temperature. Based on this method, the PD exhibited high responsivity (> 700 %) and external quantum efficiency (> 700 %). As illustrated in **Figure 10e-h**, the photo-

response speed (1 and 1.8 ms for rise and decay time, respectively) and stability are better than most of the planar perovskite PDs.

The performance of PDs can also be enhanced through scaling them down in size, thus employing low-dimensional PNC active layers.[206] Compared to 2D PNC photodetectors, the 1D PNCs (nanowires, nanobelts, and nanorods) outperform the 2D PNCs since they have less grain boundaries,[204] high crystalline quality,[212] large surface-to-volume ratio,[206] and less trap states.[212] The first research study on the 1D PDs was conducted by Horváth *et al.* using $MAPbI_3$ nanowires.[213] Though $MAPbI_3$-based 1D PNC PDs showed low photoresponsivity of 5 mA W^{-1}, excellent performance in terms of rise and decay times (less than 500 μs) were demonstrated. This result represents a $\sim 10^4$ faster photoresponse speed than that of state-of-art PDs based on monolayer MoS_2 and graphene.[213] This indicates that, by reducing the PNCs dimensions, the PD performance could be enhanced.

Another approach to significantly improve the performance of organic-inorganic 1D PNC-based PDs was through their patterning and alignment.[214] Disordered 1D PNCs may lead to poor PD performance due to the mismatch in distribution between the random nanowires and the traditional ordered electrodes. Therefore, uniform distribution, patterning and alignment of PNCs is highly desired for PDs. For example using aligned $MAPbI_3$ nanowire PDs, photoresponsivity of 1.3 A W^{-1}, which is almost 260 times larger than that in a non-aligned one, is obtained.[213,214]

As already mentioned in Section 2, fully inorganic 1D PNCs showed better stability compared to the hybrid organic-inorganic $MAPbI_3$ PNCs.[215,216] Shoaib *et al.* reported on $CsPbBr_3$ nanowire PDs with excellent responsivity up to 4.4×10^4 A W^{-1} and fast response speed of 252 μs.[215] Such high photo-responsivity could be ascribed to combination of large absorption coefficient, high charge mobility, and low trap-state density. Compared to the $CsPbBr_3$-based PDs, $CsPbI_3$-nanorod-based PDs displayed even higher performance in some aspects, such as high EQE (0.9×10^6 %) and lower rise/decay time (50/150 μs).[216] This might be due to the fact

that $MAPbI_3$ nanorods absorb more light. [217] It is worth mentioning that a PD could be stable in ambient conditions by using 1D $CsPbI_3$ nanorods as active layer. Moreover, PDs based on fully inorganic PNCs display better stability than those employing hybrid PNCs. On the other hand, the organic-inorganic PNC PDs generally show better photodetection speed compared to the fully inorganic counterparts. In fact Lian *et al.* reported ultrafast response speed of 45 ns rise and 91 ns decay times based on thin film of Cs doped $FAPbI_3$,[218] which is to the best of our knowledge the fastest times ever reported before.

5. Conclusions and future outlook

The ever-growing interest on PNCs and their fascinating optoelectronic properties makes them promising candidates for next-generation optoelectronics. PNCs possess tunable photoluminescence with high quantum yield and narrow emission bandwidth, combined to facile solution processability, inspiring the exploitation of PNCs in various device applications. In this review, we have provided a broad survey of various synthetic methods and strategies for size and morphology control of both hybrid organic/inorganic and fully inorganic metal halide PNCs in colloidal form as well as in film forms. Our review has also provided insights into addressing the two major challenges in the practical use of PNCs, namely toxicity and poor stability. The toxicity issue of PNCs can be addressed by implementing metal elements such as Sn, Ge, Bi and Sb to replace Pb. Sn-based PNCs have excellent photoelectronic properties as they absorb a broader spectrum to be better light harvesters compared to other Pb-free based PNCs. However, due to the high density of surface defects, Sn-based PNCs usually show low PLQY while suffering from the highly unstable issue mainly caused by the oxidization of Sn^{2+} to Sn^{4+} in ambient conditions. Surface passivation techniques could address the instability issue through several popular strategies, such as surface capping ligands and interfacial layers. Very recently, an alternative passivation approach to protect the unstable Sn-based perovskites has been reported.[219] In this work, by alloying Sn with Ge, an ultrathin (about 5 nm) native-oxide layer is formed on top of the perovskite surface, thus protecting it and overcoming its typical

instability problems. In addition, lead-free double or triple halide perovskites may afford a new direction to solve both toxicity and stability issues at the same time. They feature high intrinsic thermal and photo-stability, and less sensitivity to moisture, but they usually possess large bandgaps, which is harmful for photovoltaic applications. Hence, there is an urgent need of extensive bandgap engineering to make double or triple perovskite nanomaterials suitable for device applications. As another crucial point in this review, the dimensionality of PNCs has been also discussed. Recent studies have proved that the optical properties of PNCs are strongly dependent on their dimensions. Fine-tuning of PNCs' dimensions and characterization will be a key task for fully understanding the structure-property-function relationship.

As regards to the characterization methods for PNCs, the study of PNC photophysics can play a fundamental role in evaluating the peculiar behaviors of PNCs, and in supplying critical hints for their potential application in optoelectronic devices. As mentioned in Section 3 of this review, the photophysical properties of major interest include the optical properties, PLQY, and charge-carrier dynamics. A comparison between the key photophysical properties of PNCs and those of the corresponding bulk perovskite materials (**Table 6**) allows revealing the root causes behind the poorer performance in device applications of PNCs with respect to the bulk films. PNCs present tunable optical properties with relatively higher PLQY compared to bulk films, due to the characteristics of size-tuning and quantum confinement effect in PNCs not available in bulk films. In fact, these features allow PNCs to act as an efficient light absorber or emitter in solar cells and LEDs applications, respectively. The charge-carrier dynamics strongly depends on the material characteristics, including particle size, shape, crystallinity, morphology, for PNCs and bulk films as well.[95] Both nano and bulk crystals can achieve relatively long exciton lifetimes, up to several hundreds of nanoseconds in average, paving the way to efficient charge transport particularly for photon-to-current or current-to-photon applications. However, due to the extremely large surface-to-volume ratio of PNCs and accompanied surface defects, the actual charge extraction and charge transfer processes are dramatically hindered in PNCs,

resulting in lower charge separation efficiency and charge collection efficiency for PNCs, which could effectively explain why perovskite bulk films lead to much higher PCE than PNCs in solar cells applications. On the other hand, due to the size limitation in PNCs, the charge diffusion length is effectively shortened within nanometer distance compared to the long charge diffusion lengths even at micrometer level in bulk films, leading to enhanced charge recombination before the charges are collected at the respective electrodes in PNCs-based devices. Accordingly, it is crucial to improve the photophysical properties of PNCs for future device development, *i.e.* charge-carrier dynamics, to realize efficient charge extraction and swift charge transfer, similarly to conventional perovskite bulk films. Hence, we conclude that the assessment of PNCs photophysical properties can not only merely define their optoelectronic characteristics in both steady-state and kinetic mode but can especially provide an effective shortcut to the prediction of the device performance.

Regarding the various applications of PNCs, we outlined their potential role in LEDs, solar cells, lasers, and PDs. In the case of LEDs, PNCs afford super-saturated colors and high PLQY, allowing them to be an attractive and competitive class of nanomaterials. If adopted in solar cells, PNCs in low dimensions like QDs exhibit much better stability in ambient conditions, providing a tangible way to foresee PNC technology in the photovoltaic market. As regards to lasers and PDs, their performances extensively depend on the structure, composition, and morphology of the photoactive layers, indicating that PNCs are highly suitable for those applications. Considering the skyrocketing number of publications in the latest years, the coming blueprint looks bright for PNCs. All issues related to shortcomings of PNCs deserve more attention in the future for the development of PNC-based optoelectronics. In conclusion, we are convinced that the collaborative efforts from interdisciplinary scientists will advance and boost the field of perovskite nanocrystals, eventually towards their commercialization.

Acknowledgements

P.V. and M.L. acknowledge Jane & Aatos Erkko foundation (project 'ASPIRE') and Business Finland (project 'SolarWAVE') for financial support. R.N. and S.G.C. acknowledge NSERC for individual Discovery grants. This work is part of the Academy of Finland Flagship Programme, Photonics Research and Innovation (PREIN), decision 320165.

Received: ((will be filled in by the editorial staff))
Revised: ((will be filled in by the editorial staff))
Published online: ((will be filled in by the editorial staff))

References

[1] Z. Liu, J. Hu, H. Jiao, L. Li, G. Zheng, Y. Chen, Y. Huang, Q. Zhang, C. Shen, Q. Chen, H. Zhou, *Adv. Mater.* **2017**, *29*, 1606774.

[2] R. Yang, R. Li, Y. Cao, Y. Wei, Y. Miao, W. L. Tan, X. Jiao, H. Chen, L. Zhang, Q. Chen, H. Zhang, W. Zou, Y. Wang, M. Yang, C. Yi, N. Wang, F. Gao, C. R. McNeill, T. Qin, J. Wang, W. Huang, *Adv. Mater.* **2018**, *30*, 1804771.

[3] N. J. Jeon, H. Na, E. H. Jung, T.-Y. Yang, Y. G. Lee, G. Kim, H.-W. Shin, S. Il Seok, J. Lee, J. Seo, *Nat. Energy* **2018**, *3*, 682.

[4] Y. Dong, Y. Zhao, S. Zhang, Y. Dai, L. Liu, Y. Li, Q. Chen, *J. Mater. Chem. A* **2018**, *6*, 21729.

[5] J. Song, J. Li, X. Li, L. Xu, Y. Dong, H. Zeng, *Adv. Mater.* **2015**, *27*, 7162.

[6] H. Cho, S.-H. Jeong, M.-H. Park, Y.-H. Kim, C. Wolf, C.-L. Lee, J. H. Heo, A. Sadhanala, N. Myoung, S. Yoo, S. H. Im, R. H. Friend, T.-W. Lee, *Science* **2015**, *350*, 1222.

[7] P. Liu, X. He, J. Ren, Q. Liao, J. Yao, H. Fu, *ACS Nano* **2017**, *11*, 5766.

[8] R. Yan, D. Gargas, P. Yang, *Nat. Photonics* **2009**, *3*, 569.

[9] H. Zhou, J. Zeng, Z. Song, C. R. Grice, C. Chen, Z. Song, D. Zhao, H. Wang, Y. Yan, *J. Phys. Chem. Lett.* **2018**, *9*, 2043.

[10] J. H. Noh, S. H. Im, J. H. Heo, T. N. Mandal, S. Il Seok, *Nano Lett.* **2013**, *13*, 1764.

[11] N. Kitazawa, Y. Watanabe, Y. Nakamura, *J. Mater. Sci.* **2002**, *37*, 3585.

[12] C. C. Stoumpos, C. D. Malliakas, M. G. Kanatzidis, *Inorg. Chem.* **2013**, *52*, 9019.

[13] V. D'Innocenzo, G. Grancini, M. J. P. Alcocer, A. R. S. Kandada, S. D. Stranks, M. M.

Lee, G. Lanzani, H. J. Snaith, A. Petrozza, *Nat. Commun.* **2014**, *5*, 3586.

[14] K. W. Tan, D. T. Moore, M. Saliba, H. Sai, L. A. Estroff, T. Hanrath, H. J. Snaith, U. Wiesner, *ACS Nano* **2014**, *8*, 4730.

[15] N. K. Noel, S. D. Stranks, A. Abate, C. Wehrenfennig, S. Guarnera, A.-A. Haghighirad, A. Sadhanala, G. E. Eperon, S. K. Pathak, M. B. Johnston, A. Petrozza, L. M. Herz, H. J. Snaith, *Energy Environ. Sci.* **2014**, *7*, 3061.

[16] N. Wang, L. Cheng, R. Ge, S. Zhang, Y. Miao, W. Zou, C. Yi, Y. Sun, Y. Cao, R. Yang, Y. Wei, Q. Guo, Y. Ke, M. Yu, Y. Jin, Y. Liu, Q. Ding, D. Di, L. Yang, G. Xing, H. Tian, C. Jin, F. Gao, R. H. Friend, J. Wang, W. Huang, *Nat. Photonics* **2016**, *10*, 699.

[17] L. Zhou, Y.-F. Xu, B.-X. Chen, D.-B. Kuang, C.-Y. Su, *Small* **2018**, *14*, 1703762.

[18] X.-G. Zhao, J.-H. Yang, Y. Fu, D. Yang, Q. Xu, L. Yu, S.-H. Wei, L. Zhang, *J. Am. Chem. Soc.* **2017**, *139*, 2630.

[19] Y. Zhao, K. Zhu, *Chem. Soc. Rev.* **2016**, *45*, 655.

[20] J. Burschka, N. Pellet, S.-J. Moon, R. Humphry-Baker, P. Gao, M. K. Nazeeruddin, M. Grätzel, *Nature* **2013**, *499*, 316.

[21] M. Liu, M. B. Johnston, H. J. Snaith, *Nature* **2013**, *501*, 395.

[22] A. Veamatahau, B. Jiang, T. Seifert, S. Makuta, K. Latham, M. Kanehara, T. Teranishi and Y. Tachibana, *Phys. Chem. Chem. Phys.* **2015**, *17*, 2850.

[23] Q. Zhang, S. T. Ha, X. Liu, T. C. Sum, Q. Xiong, *Nano Lett.* **2014**, *14*, 5995.

[24] W. Nie, H. Tsai, R. Asadpour, J.-C. Blancon, A. J. Neukirch, G. Gupta, J. J. Crochet, M. Chhowalla, S. Tretiak, M. A. Alam, H.-L. Wang, A. D. Mohite, *Sci. (Washington, DC, United States)* **2015**, *347*, 522.

[25] Z.-K. Tan, R. S. Moghaddam, M. L. Lai, P. Docampo, R. Higler, F. Deschler, M. Price, A. Sadhanala, L. M. Pazos, D. Credgington, F. Hanusch, T. Bein, H. J. Snaith, R. H. Friend, *Nat. Nanotechnol.* **2014**, *9*, 687.

[26] F. Li, C. Ma, H. Wang, W. Hu, W. Yu, A. D. Sheikh, T. Wu, *Nat. Commun.* **2015**, *6*, 8238.

[27] X. Hu, X. Zhang, L. Liang, J. Bao, S. Li, W. Yang, Y. Xie, *Adv. Funct. Mater.* **2014**, *24*, 7373.

[28] Y. Zhang, J. Du, X. Wu, G. Zhang, Y. Chu, D. Liu, Y. Zhao, Z. Liang, J. Huang, *ACS Appl. Mater. Interfaces* **2015**, *7*, 21634.

[29] M. V Kovalenko, L. Protesescu, M. I. Bodnarchuk, *Science* **2017**, *358*, 745.

[30] X. He, Y. Qiu, S. Yang, *Adv. Mater.* **2017**, *29*, 1700775.

[31] X. Qi, Y. Zhang, Q. Ou, S. T. Ha, C.-W. Qiu, H. Zhang, Y.-B. Cheng, Q. Xiong, Q. Bao, *Small* **2018**, *14*, 1800682.

[32] E. A. Tsiwah, Y. Ding, Z. Li, Z. Zhao, M. Wang, C. Hu, X. Liu, C. Sun, X. Zhao, Y. Xie, *CrystEngComm* **2017**, *19*, 7041.

[33] D. M. Jang, D. H. Kim, K. Park, J. Park, J. W. Lee, J. K. Song, *J. Mater. Chem. C* **2016**, *4*, 10625.

[34] Z. Long, H. Ren, J. Sun, J. Ouyang, N. Na, *Chem. Commun.* **2017**, *53*, 9914.

[35] L. Protesescu, S. Yakunin, M. I. Bodnarchuk, F. Krieg, R. Caputo, C. H. Hendon, R. X. Yang, A. Walsh, M. V. Kovalenko, *Nano Lett.* **2015**, *15*, 3692.

[36] F. Zhang, H. Zhong, C. Chen, X. Wu, X. Hu, H. Huang, J. Han, B. Zou, Y. Dong, *ACS Nano* **2015**, *9*, 4533.

[37] L. Protesescu, S. Yakunin, O. Nazarenko, D. N. Dirin, M. V. Kovalenko, *ACS Appl. Nano Mater.* **2018**, *1*, 1300.

[38] M. I. Saidaminov, O. F. Mohammed, O. M. Bakr, *ACS Energy Lett.* **2017**, *2*, 889.

[39] V. D'Innocenzo, A. R. Srimath Kandada, M. De Bastiani, M. Gandini, A. Petrozza, *J. Am. Chem. Soc.* **2014**, *136*, 17730.

[40] N. K. Noel, A. Abate, S. D. Stranks, E. S. Parrott, V. M. Burlakov, A. Goriely, H. J. Snaith, *ACS Nano* **2014**, *8*, 9815.

[41] L. C. Schmidt, A. Pertegás, S. González-Carrero, O. Malinkiewicz, S. Agouram, G. Mínguez Espallargas, H. J. Bolink, R. E. Galian, J. Pérez-Prieto, *J. Am. Chem. Soc.* **2014**, *136*, 850.

[42] W. Tian, C. Zhao, J. Leng, R. Cui, S. Jin, *J. Am. Chem. Soc.* **2015**, *137*, 12458.

[43] J. A. Sichert, Y. Tong, N. Mutz, M. Vollmer, S. Fischer, K. Z. Milowska, R. García Cortadella, B. Nickel, C. Cardenas-Daw, J. K. Stolarczyk, A. S. Urban, J. Feldmann, *Nano Lett.* **2015**, *15*, 6521.

[44] S. Sun, D. Yuan, Y. Xu, A. Wang, Z. Deng, *ACS Nano* **2016**, *10*, 3648.

[45] Y.-F. Xu, M.-Z. Yang, B.-X. Chen, X.-D. Wang, H.-Y. Chen, D.-B. Kuang, C.-Y. Su, *J. Am. Chem. Soc.* **2017**, *139*, 5660.

[46] Y. Zhang, J. Liu, Z. Wang, Y. Xue, Q. Ou, L. Polavarapu, J. Zheng, X. Qi, Q. Bao, *Chem. Commun.* **2016**, *52*, 13637.

[47] H. Ma, M. Imran, Z. Dang, Z. Hu, H. H. Ma, M. Imran, Z. Dang, Z. Hu, *Crystals* **2018**, *8*, 182.

[48] Q. A. Akkerman, G. Rainò, M. V. Kovalenko, L. Manna, *Nat. Mater.* **2018**, *17*, 394.

[49] H. Huang, A. S. Susha, S. V. Kershaw, T. F. Hung, A. L. Rogach, *Adv. Sci.* **2015**, *2*, 1500194.

[50] S. Chan, M. Liu, K. Latham, M. Haruta, H. Kurata, T. Teranishi, Y. Tachibana, *J. Mater. Chem. C* **2017**, *5*, 2182.

[51] C. Tanford, *J. Phys. Chem.* **1974**, *78*, 2469.

[52] J. Eastoe, M. J. Hollamby, L. Hudson, *Adv. Colloid Interface Sci.* **2006**, *128–130*, 5.

[53] A. Pan, B. He, X. Fan, Z. Liu, J. J. Urban, A. P. Alivisatos, L. He, Y. Liu, *ACS Nano* **2016**, *10*, 7943.

[54] M. Imran, V. Caligiuri, M. Wang, L. Goldoni, M. Prato, R. Krahne, L. De Trizio, L. Manna, *J. Am. Chem. Soc.* **2018**, *140*, 2656.

[55] B. Xin, Y. Pak, S. Mitra, D. Almalawi, N. Alwadai, Y. Zhang, I. S. Roqan, S. Arabia,

2019, *11*, 5223.

[56] D. M. Jang, K. Park, D. H. Kim, J. Park, F. Shojaei, H. S. Kang, J.-P. Ahn, J. W. Lee, J. K. Song, *Nano Lett.* **2015**, *15*, 5191.

[57] Q. A. Akkerman, V. D'Innocenzo, S. Accornero, A. Scarpellini, A. Petrozza, M. Prato, L. Manna, *J. Am. Chem. Soc.* **2015**, *137*, 10276.

[58] G. Li, J. Y.-L. Ho, M. Wong, H. S. Kwok, *J. Phys. Chem. C* **2015**, *119*, 26883.

[59] A. B. Wong, M. Lai, S. W. Eaton, Y. Yu, E. Lin, L. Dou, A. Fu, P. Yang, *Nano Lett.* **2015**, *15*, 5519.

[60] D. Zhang, Y. Yang, Y. Bekenstein, Y. Yu, N. A. Gibson, A. B. Wong, S. W. Eaton, N. Kornienko, Q. Kong, M. Lai, A. P. Alivisatos, S. R. Leone, P. Yang, *J. Am. Chem. Soc.* **2016**, *138*, 7236.

[61] J. B. Hoffman, A. L. Schleper, P. V. Kamat, *J. Am. Chem. Soc.* **2016**, *138*, 8603.

[62] D. Parobek, Y. Dong, T. Qiao, D. Rossi, D. H. Son, *J. Am. Chem. Soc.* **2017**, *139*, 4358.

[63] K. Chen, X. Deng, R. Goddard, H. Tüysüz, *Chem. Mater.* **2016**, *28*, 5530.

[64] W. van der Stam, J. J. Geuchies, T. Altantzis, K. H. W. van den Bos, J. D. Meeldijk, S. Van Aert, S. Bals, D. Vanmaekelbergh, C. de Mello Donega, *J. Am. Chem. Soc.* **2017**, *139*, 4087.

[65] L. Protesescu, S. Yakunin, S. Kumar, J. Bär, F. Bertolotti, N. Masciocchi, A. Guagliardi, M. Grotevent, I. Shorubalko, M. I. Bodnarchuk, C.-J. Shih, M. V. Kovalenko, *ACS Nano* **2017**, *11*, 3119.

[66] L. Qiu, L. K. Ono, Y. Qi, *Mater. Today Energy* **2018**, *7*, 169.

[67] B. Yang, X. Mao, F. Hong, W. Meng, Y. Tang, X. Xia, S. Yang, W. Deng, K. Han, *J. Am. Chem. Soc.* **2018**, *140*, 17001.

[68] S. E. Creutz, E. N. Crites, M. C. De Siena, D. R. Gamelin, *Nano Lett.* **2018**, *18*, 1118.

[69] B. Yang, J. Chen, F. Hong, X. Mao, K. Zheng, S. Yang, Y. Li, T. Pullerits, W. Deng,

K. Han, *Angew. Chem. Int. Ed. Engl.* **2017**, *56*, 12471.

[70] F. Giustino, H. J. Snaith, *ACS Energy Lett.* **2016**, *1*, 1233.

[71] M. Lyu, J.-H. Yun, P. Chen, M. Hao, L. Wang, *Adv. Energy Mater.* **2017**, *7*, 1602512.

[72] Z. Shi, J. Guo, Y. Chen, Q. Li, Y. Pan, H. Zhang, Y. Xia, W. Huang, *Adv. Mater.* **2017**, *29*, 1605005.

[73] S. F. Hoefler, G. Trimmel, T. Rath, *Monatshefte für Chemie - Chem. Mon.* **2017**, *148*, 795.

[74] N. Rajeev Kumar, R. Radhakrishnan, *Mater. Lett.* **2018**, *227*, 289.

[75] A. Jain, O. Voznyy, E. H. Sargent, *J. Phys. Chem. C* **2017**, *18*, 28.

[76] S. Lu, Q. Zhou, Y. Ouyang, Y. Guo, Q. Li, J. Wang, *Nat. Commun.* **2018**, *9*, 3405.

[77] M. Pazoki, T. Edvinsson, *Sustain. Energy Fuels* **2018**, *2*, 1430.

[78] J. Sun, J. Yang, J. I. Lee, J. H. Cho, M. S. Kang, *J. Phys. Chem. Lett.* **2018**, *9*, 1573.

[79] K. Yamada, H. Kawaguchi, T. Matsui, T. Okuda, S. Ichiba, *Bull. Chem. Soc. Jpn.* **1990**, *63*, 2521.

[80] S. Shao, J. Liu, G. Portale, H.-H. Fang, G. R. Blake, G. H. ten Brink, L. J. A. Koster, M. A. Loi, *Adv. Energy Mater.* **2018**, *8*, 1702019.

[81] A. Babayigit, A. Ethirajan, M. Muller, B. Conings, *Nat. Mater.* **2016**, *15*, 247.

[82] M. Konstantakou, T. Stergiopoulos, **2017**, *5*, 11518.

[83] M. Leng, Z. Chen, Y. Yang, Z. Li, K. Zeng, K. Li, G. Niu, Y. He, Q. Zhou, J. Tang, *Angew. Chemie Int. Ed.* **2016**, *55*, 15012.

[84] R. D. Nelson, K. Santra, Y. Wang, A. Hadi, J. W. Petrich, M. G. Panthani, *Chem. Commun.* **2018**, *54*, 3640.

[85] Z. Xiao, W. Meng, J. Wang, D. B. Mitzi, Y. Yan, *Mater. Horizons* **2017**, *4*, 206.

[86] K. Kihara, T. Sudo, *Zeitschrift für Krist. - Cryst. Mater.* **1971**, *134*, 142.

[87] K. Kihara, T. Sudo, IUCr, *Acta Crystallogr. Sect. B Struct. Crystallogr. Cryst. Chem.* **1974**, *30*, 1088.

[88] B. Saparov, F. Hong, J.-P. Sun, H.-S. Duan, W. Meng, S. Cameron, I. G. Hill, Y. Yan, D. B. Mitzi, *Chem. Mater.* **2015**, *27*, 5622.

[89] C. Zuo, L. Ding, *Angew. Chemie Int. Ed.* **2017**, *56*, 6528.

[90] J.-C. Hebig, I. Kühn, J. Flohre, T. Kirchartz, *ACS Energy Lett.* **2016**, *1*, 309.

[91] J. Zhang, Y. Yang, H. Deng, U. Farooq, X. Yang, J. Khan, J. Tang, H. Song, *ACS Nano* **2017**, *11*, 9294.

[92] V. M. Goldschmidt, V. M., *Naturwissenschaften* **1926**, *14*, 477.

[93] H.-S. Kim, S. H. Im, N.-G. Park, *J. Phys. Chem. C* **2014**, *118*, 5615.

[94] G. Volonakis, † Amir, A. Haghighirad, R. L. Milot, W. H. Sio, M. R. Filip, B. Wenger, M. B. Johnston, L. M. Herz, H. J. Snaith, F. Giustino, *J. Phys. Chem. Lett* **2017**, *8*, 52.

[95] S. Bonabi Naghadeh, B. Luo, G. Abdelmageed, Y.-C. Pu, C. Zhang, J. Z. Zhang, *J. Phys. Chem. C* **2018**, *122*, 15799.

[96] V. K. Ravi, G. B. Markad, A. Nag, *ACS Energy Lett.* **2016**, *1*, 665.

[97] S. Yakunin, L. Protesescu, F. Krieg, M. I. Bodnarchuk, G. Nedelcu, M. Humer, G. De Luca, M. Fiebig, W. Heiss, M. V. Kovalenko, *Nat. Commun.* **2015**, *6*, 8056.

[98] A. Filippetti, A. Mattoni, *Phys. Rev. B* **2014**, *89*, 125203.

[99] D. Yang, X. Li, H. Zeng, *Adv. Mater. Interfaces* **2018**, *5*, 1701662.

[100] J. De Roo, M. Ibáñez, P. Geiregat, G. Nedelcu, W. Walravens, J. Maes, J. C. Martins, I. Van Driessche, M. V. Kovalenko, Z. Hens, *ACS Nano* **2016**, *10*, 2071.

[101] B. Luo, S. B. Naghadeh, A. Allen, X. Li, J. Z. Zhang, *Adv. Funct. Mater.* **2017**, *27*, 1604018.

[102] C. Wang, A. S. R. Chesman, J. J. Jasieniak, *Chem. Commun.* **2017**, *53*, 232.

[103] V. K. Ravi, R. A. Scheidt, A. Nag, M. Kuno, P. V. Kamat, *ACS Energy Lett.* **2018**, *3*, 1049.

[104] F. Krieg, S. T. Ochsenbein, S. Yakunin, S. ten Brinck, P. Aellen, A. Süess, B. Clerc, D. Guggisberg, O. Nazarenko, Y. Shynkarenko, S. Kumar, C.-J. Shih, I. Infante, M. V.

Kovalenko, *ACS Energy Lett.* **2018**, *3*, 641.

[105] B. Luo, Y.-C. Pu, S. A. Lindley, Y. Yang, L. Lu, Y. Li, X. Li, J. Z. Zhang, *Angew. Chemie Int. Ed.* **2016**, *55*, 8864.

[106] S. Seth, A. Samanta, *Sci. Rep.* **2016**, *6*, 37693.

[107] C. Wang, Y. Zhang, A. Wang, Q. Wang, H. Tang, W. Shen, Z. Li, Z. Deng, *Chem. Mater.* **2017**, *29*, 2157.

[108] G. Niu, X. Guo, L. Wang, *J. Mater. Chem. A* **2015**, *3*, 8970.

[109] O. Vybornyi, S. Yakunin, M. V. Kovalenko, *Nanoscale* **2016**, *8*, 6278.

[110] I. M. Asuo, P. Fourmont, I. Ka, D. Gedamu, S. Bouzidi, A. Pignolet, R. Nechache, S. G. Cloutier, *Small* **2019**, *15*, 1804150.

[111] H. Yuan, E. Debroye, K. Janssen, H. Naiki, C. Steuwe, G. Lu, M. Moris, E. Orgiu, H. Uji-i, F. De Schryver, P. Samorì, J. Hofkens, M. Roeffaers, *J. Phys. Chem. Lett.* **2016**, *7*, 561.

[112] I. M. Asuo, D. Gedamu, I. Ka, L. F. Gerlein, F.-X. Fortier, A. Pignolet, S. G. Cloutier, R. Nechache, *Nano Energy* **2018**, *51*, 324.

[113] F. Palazon, F. Di Stasio, Q. A. Akkerman, R. Krahne, M. Prato, L. Manna, *Chem. Mater.* **2016**, *28*, 2902.

[114] J. Li, L. Wang, X. Yuan, B. Bo, H. Li, J. Zhao, X. Gao, *Mater. Res. Bull.* **2018**, *102*, 86.

[115] J. Li, B. Bo, X. Gao, **2018**, *2036*, 30018.

[116] M. Ouafi, B. Jaber, L. Atourki, R. Bekkari, L. Laânab, *J. Alloys Compd.* **2018**, *746*, 391.

[117] T. Zou, X. Liu, R. Qiu, Y. Wang, S. Huang, C. Liu, Q. Dai, H. Zhou, *Adv. Opt. Mater.* **2019**, 1801812.

[118] Q. Wang, N. Phung, D. Di Girolamo, P. Vivo, A. Abate, *Energy Environ. Sci.* **2019**, *7*, 703.

[119] A. Farooq, I. M. Hossain, S. Moghadamzadeh, J. A. Schwenzer, T. Abzieher, B. S. Richards, E. Klampaftis, U. W. Paetzold, *ACS Appl. Mater. Interfaces* **2018**, *10*, 21985.

[120] F. Huang, L. Jiang, A. R. Pascoe, Y. Yan, U. Bach, L. Spiccia, Y.-B. Cheng, *Nano Energy* **2016**, *27*, 509.

[121] M. V. Khenkin, A. K. M., I. Visoly-Fisher, Y. Galagan, F. Di Giacomo, B. R. Patil, G. Sherafatipour, V. Turkovic, H.-G. Rubahn, M. Madsen, T. Merckx, G. Uytterhoeven, J. P. A. Bastos, T. Aernouts, F. Brunetti, M. Lira-Cantu, E. A. Katz, *Energy Environ. Sci.* **2018**, *11*, 739.

[122] H. Huang, M. I. Bodnarchuk, S. V Kershaw, M. V Kovalenko, A. L. Rogach, *ACS Energy Lett.* **2017**, *2*, 2071.

[123] W. Chen, J. Hao, W. Hu, Z. Zang, X. Tang, L. Fang, T. Niu, M. Zhou, *Small* **2017**, *13*, 1604085.

[124] F. Liu, Y. Zhang, C. Ding, S. Kobayashi, T. Izuishi, N. Nakazawa, T. Toyoda, T. Ohta, S. Hayase, T. Minemoto, K. Yoshino, S. Dai, Q. Shen, *ACS Nano* **2017**, *11*, 10373.

[125] T. C. Jellicoe, J. M. Richter, H. F. J. Glass, M. Tabachnyk, R. Brady, S. E. Dutton, A. Rao, R. H. Friend, D. Credgington, N. C. Greenham, M. L. Böhm, *J. Am. Chem. Soc.* **2016**, *138*, 2941.

[126] X. Li, M. I. Dar, C. Yi, J. Luo, M. Tschumi, S. M. Zakeeruddin, M. K. Nazeeruddin, H. Han, M. Grätzel, **2015**, DOI 10.1038/NCHEM.2324.

[127] A. Binek, F. C. Hanusch, P. Docampo, T. Bein, *J. Phys. Chem. Lett.* **2015**, *6*, 1249.

[128] G. E. Eperon, S. D. Stranks, C. Menelaou, M. B. Johnston, L. M. Herz, H. J. Snaith, *Energy Environ. Sci.* **2014**, *7*, 982.

[129] G. Nedelcu, L. Protesescu, S. Yakunin, M. I. Bodnarchuk, M. J. Grotevent, M. V. Kovalenko, *Nano Lett.* **2015**, *15*, 5635.

[130] D. Zhang, S. W. Eaton, Y. Yu, L. Dou, P. Yang, *J. Am. Chem. Soc.* **2015**, *137*, 9230.

[131] Q. A. Akkerman, S. G. Motti, A. R. Srimath Kandada, E. Mosconi, V. D'Innocenzo, G.

Bertoni, S. Marras, B. A. Kamino, L. Miranda, F. De Angelis, A. Petrozza, M. Prato, L. Manna, *J. Am. Chem. Soc.* **2016**, *138*, 1010.

[132] Y. Bekenstein, B. A. Koscher, S. W. Eaton, P. Yang, A. P. Alivisatos, *J. Am. Chem. Soc.* **2015**, *137*, 16008.

[133] L. Ma, F. Hao, C. C. Stoumpos, B. T. Phelan, M. R. Wasielewski, M. G. Kanatzidis, *J. Am. Chem. Soc.* **2016**, *138*, 14750.

[134] A. B. Wong, Y. Bekenstein, J. Kang, C. S. Kley, D. Kim, N. A. Gibson, D. Zhang, Y. Yu, S. R. Leone, L.-W. Wang, A. P. Alivisatos, P. Yang, *Nano Lett.* **2018**, *18*, 2060.

[135] A. Wang, X. Yan, M. Zhang, S. Sun, M. Yang, W. Shen, X. Pan, P. Wang, Z. Deng, *Chem. Mater.* **2016**, *28*, 8132.

[136] M. Leng, Y. Yang, K. Zeng, Z. Chen, Z. Tan, S. Li, J. Li, B. Xu, D. Li, M. P. Hautzinger, Y. Fu, T. Zhai, L. Xu, G. Niu, S. Jin, J. Tang, *Adv. Funct. Mater.* **2018**, *28*, 1704446.

[137] J. Pal, S. Manna, A. Mondal, S. Das, K. V. Adarsh, A. Nag, *Angew. Chemie Int. Ed.* **2017**, *56*, 14187.

[138] K. Du, W. Meng, X. Wang, Y. Yan, D. B. Mitzi, *Angew. Chemie Int. Ed.* **2017**, *56*, 8158.

[139] E. T. McClure, M. R. Ball, W. Windl, P. M. Woodward, *Chem. Mater.* **2016**, *28*, 1348.

[140] G. Volonakis, A. A. Haghighirad, R. L. Milot, W. H. Sio, M. R. Filip, B. Wenger, M. B. Johnston, L. M. Herz, H. J. Snaith, F. Giustino, *J. Phys. Chem. Lett.* **2017**, *8*, 772.

[141] B. Vargas, E. Ramos, E. Pérez-Gutiérrez, J. C. Alonso, D. Solis-Ibarra, *J. Am. Chem. Soc.* **2017**, *139*, 9116.

[142] D. Zhao, Y. Yu, C. Wang, W. Liao, N. Shrestha, C. R. Grice, A. J. Cimaroli, L. Guan, R. J. Ellingson, K. Zhu, X. Zhao, R.-G. Xiong, Y. Yan, *Nat. Energy* **2017**, *2*, 17018.

[143] R. A. Scheidt, G. F. Samu, C. Janáky, P. V. Kamat, *J. Am. Chem. Soc.* **2018**, *140*, 86.

[144] S. D. Stranks, G. E. Eperon, G. Grancini, C. Menelaou, M. J. P. Alcocer, T. Leijtens, L.

M. Herz, A. Petrozza, H. J. Snaith, *Science* **2013**, *342*, 341.

[145] L. Lv, Y. Xu, H. Fang, W. Luo, F. Xu, L. Liu, B. Wang, X. Zhang, D. Yang, W. Hu, A. Dong, *Nanoscale* **2016**, *8*, 13589.

[146] B. Luo, Y.-C. Pu, Y. Yang, S. A. Lindley, G. Abdelmageed, H. Ashry, Y. Li, X. Li, J. Z. Zhang, *J. Phys. Chem. C* **2015**, *119*, 26672.

[147] E. M. Hutter, M. C. Gélvez-Rueda, A. Osherov, V. Bulović, F. C. Grozema, S. D. Stranks, T. J. Savenije, *Nat. Mater.* **2017**, *16*, 115.

[148] C. Motta, F. El-Mellouhi, S. Kais, N. Tabet, F. Alharbi, S. Sanvito, *Nat. Commun.* **2015**, *6*, 7026.

[149] F. Zheng, L. Z. Tan, S. Liu, A. M. Rappe, *Nano Lett.* **2015**, *15*, 7794.

[150] T. Etienne, E. Mosconi, F. De Angelis, *J. Phys. Chem. Lett.* **2016**, *7*, 1638.

[151] Y. Zhang, J. Yin, M. R. Parida, G. H. Ahmed, J. Pan, O. M. Bakr, J.-L. Brédas, O. F. Mohammed, *J. Phys. Chem. Lett.* **2017**, *8*, 3173.

[152] K. M. McCall, C. C. Stoumpos, S. S. Kostina, M. G. Kanatzidis, B. W. Wessels, *Chem. Mater.* **2017**, *29*, 4129.

[153] X. Wen, L. Van Dao, P. Hannaford, *J. Phys. D. Appl. Phys.* **2007**, *40*, 3573.

[154] M. Liu, Y. Tachibana, *J. Phys. Chem. Lett.* **2019**, under review.

[155] J. Dai, Y. Fu, L. H. Manger, M. T. Rea, L. Hwang, R. H. Goldsmith, S. Jin, *J. Phys. Chem. Lett.* **2016**, *7*, 5036.

[156] Z. Tan, J. Li, C. Zhang, Z. Li, Q. Hu, Z. Xiao, T. Kamiya, H. Hosono, G. Niu, E. Lifshitz, Y. Cheng, J. Tang, *Adv. Funct. Mater.* **2018**, *28*, 1801131.

[157] R. J. Sutton, G. E. Eperon, L. Miranda, E. S. Parrott, B. A. Kamino, J. B. Patel, M. T. Hörantner, M. B. Johnston, A. A. Haghighirad, D. T. Moore, H. J. Snaith, *Adv. Energy Mater.* **2016**, *6*, 1502458.

[158] L. Polavarapu, B. Nickel, J. Feldmann, A. S. Urban, *Adv. Energy Mater.* **2017**, *7*, 1700267.

[159] T. Franzl, T. A. Klar, S. Schietinger, . A. L. Rogach, J. Feldmann, **2004**, *4*, 1599.

[160] G. Li, F. W. R. Rivarola, N. J. L. K. Davis, S. Bai, T. C. Jellicoe, F. de la Peña, S. Hou, C. Ducati, F. Gao, R. H. Friend, N. C. Greenham, Z.-K. Tan, *Adv. Mater.* **2016**, *28*, 3528.

[161] X. Zhang, H. Lin, H. Huang, C. Reckmeier, Y. Zhang, W. C. H. Choy, A. L. Rogach, *Nano Lett.* **2016**, *16*, 1415.

[162] A. Yangui, D. Garrot, J. S. Lauret, A. Lusson, G. Bouchez, E. Deleporte, S. Pillet, E. E. Bendeif, M. Castro, S. Triki, Y. Abid, K. Boukheddaden, *J. Phys. Chem. C* **2015**, *119*, 23638.

[163] S. Pathak, N. Sakai, F. Wisnivesky Rocca Rivarola, S. D. Stranks, J. Liu, G. E. Eperon, C. Ducati, K. Wojciechowski, J. T. Griffiths, A. A. Haghighirad, A. Pellaroque, R. H. Friend, H. J. Snaith, *Chem. Mater.* **2015**, *27*, 8066.

[164] J. M. Richter, M. Abdi-Jalebi, A. Sadhanala, M. Tabachnyk, J. P. H. Rivett, L. M. Pazos-Outón, K. C. Gödel, M. Price, F. Deschler, R. H. Friend, *Nat. Commun.* **2016**, *7*, 13941.

[165] O. A. Jaramillo-Quintero, R. S. Sanchez, M. Rincon, I. Mora-Sero, *J. Phys. Chem. Lett.* **2015**, *6*, 1883.

[166] L. Gil-Escrig, G. Longo, A. Pertegás, C. Roldán-Carmona, A. Soriano, M. Sessolo, H. J. Bolink, *Chem. Commun.* **2015**, *51*, 569.

[167] J. C. Yu, D. Bin Kim, G. Baek, B. R. Lee, E. D. Jung, S. Lee, J. H. Chu, D.-K. Lee, K. J. Choi, S. Cho, M. H. Song, *Adv. Mater.* **2015**, *27*, 3492.

[168] B. Lee, C. C. Stoumpos, N. Zhou, F. Hao, C. Malliakas, C.-Y. Yeh, T. J. Marks, M. G. Kanatzidis, R. P. H. Chang, **2014**, *136*, 15379.

[169] Y. Ling, Z. Yuan, Y. Tian, X. Wang, J. C. Wang, Y. Xin, K. Hanson, B. Ma, H. Gao, *Adv. Mater.* **2016**, *28*, 305.

[170] S. Wang, Y. Jiang, E. J. Juarez-Perez, L. K. Ono, Y. Qi, *Nat. Energy* **2017**, *2*, 16195.

[171] E. J. Juarez-Perez, Z. Hawash, S. R. Raga, L. K. Ono, Y. Qi, *Energy Environ. Sci.* **2016**, *9*, 3406.

[172] H. Cho, C. Wolf, J. S. Kim, H. J. Yun, J. S. Bae, H. Kim, J.-M. Heo, S. Ahn, T.-W. Lee, *Adv. Mater.* **2017**, *29*, 1700579.

[173] H.-K. Seo, H. Kim, J. Lee, M.-H. Park, S.-H. Jeong, Y.-H. Kim, S.-J. Kwon, T.-H. Han, S. Yoo, T.-W. Lee, *Adv. Mater.* **2017**, *29*, 1605587.

[174] H. Kim, A. Hagfeldt, N. Park, *Chem. Commun.* **2019**, *55*, 1192.

[175] A. Swarnkar, A. R. Marshall, E. M. Sanehira, B. D. Chernomordik, D. T. Moore, J. A. Christians, T. Chakrabarti, J. M. Luther, *Science* **2016**, *354*, 92.

[176] J.-H. Im, J. Luo, M. Franckevičius, N. Pellet, P. Gao, T. Moehl, S. M. Zakeeruddin, M. K. Nazeeruddin, M. Grätzel, N.-G. Park, *Nano Lett.* **2015**, *15*, 2120.

[177] E. M. Sanehira, A. R. Marshall, J. A. Christians, S. P. Harvey, P. N. Ciesielski, L. M. Wheeler, P. Schulz, L. Y. Lin, M. C. Beard, J. M. Luther, *Sci. Adv.* **2017**, *3*, 4204.

[178] H. Bian, D. Bai, Z. Jin, K. Wang, L. Liang, H. Wang, J. Zhang, Q. Wang, S. (Frank) Liu, *Joule* **2018**, *2*, 1500.

[179] R. Soltani, B. M. D. Puscher, A. A. Katbab, I. Levchuk, N. Kazerouni, N. Gasparini, N. Camaioni, A. Osvet, M. Batentschuk, R. H. Fink, D. M. Guldi, T. Ameri, *Phys. Chem. Chem. Phys.* **2018**, *20*, 23674.

[180] J. Zhang, D. Bai, Z. Jin, H. Bian, K. Wang, J. Sun, Q. Wang, S. F. Liu, *Adv. Energy Mater.* **2018**, *8*, 1870067.

[181] Y. Guo, K. Shoyama, W. Sato, E. Nakamura, *Adv. Energy Mater.* **2016**, *6*, 1502317.

[182] Q. Wang, Z. Jin, D. Chen, D. Bai, H. Bian, J. Sun, G. Zhu, G. Wang, S. F. Liu, *Adv. Energy Mater.* **2018**, *8*, 1800007.

[183] L. M. Wheeler, E. M. Sanehira, A. R. Marshall, P. Schulz, M. Suri, N. C. Anderson, J. A. Christians, D. Nordlund, D. Sokaras, T. Kroll, S. P. Harvey, J. J. Berry, L. Y. Lin, J. M. Luther, *J. Am. Chem. Soc.* **2018**, *140*, 10504.

[184] J. Xue, J.-W. Lee, Z. Dai, R. Wang, S. Nuryyeva, M. E. Liao, S.-Y. Chang, L. Meng, D. Meng, P. Sun, O. Lin, M. S. Goorsky, Y. Yang, *Joule* **2018**, *2*, 1866.

[185] J. Yuan, X. Ling, D. Yang, F. Li, S. Zhou, J. Shi, Y. Qian, J. Hu, Y. Sun, Y. Yang, X. Gao, S. Duhm, Q. Zhang, W. Ma, *Joule* **2018**, *2*, 2450.

[186] G. Xing, N. Mathews, S. S. Lim, N. Yantara, X. Liu, D. Sabba, M. Grätzel, S. Mhaisalkar, T. C. Sum, *Nat. Mater.* **2014**, *13*, 476.

[187] Z. Li, J. Moon, A. Gharajeh, R. Haroldson, R. Hawkins, W. Hu, A. Zakhidov, Q. Gu, *ACS Nano* **2018**, *12*, 10968.

[188] S. Yakunin, L. Protesescu, F. Krieg, M. I. Bodnarchuk, G. Nedelcu, M. Humer, G. De Luca, M. Fiebig, W. Heiss, M. V Kovalenko, *Nat. Commun.* **2015**, *6*, 8056.

[189] Y. Wang, X. Li, J. Song, L. Xiao, H. Zeng, H. Sun, *Adv. Mater.* **2015**, *27*, 7101.

[190] Y. Wang, X. Li, V. Nalla, H. Zeng, H. Sun, *Adv. Funct. Mater.* **2017**, *27*, 1605088.

[191] C.-Y. Huang, C. Zou, C. Mao, K. L. Corp, Y.-C. Yao, Y.-J. Lee, C. W. Schlenker, A. K. Y. Jen, L. Y. Lin, *ACS Photonics* **2017**, *4*, 2281.

[192] C. H. Lin, Q. Zeng, E. Lafalce, S. Yu, M. J. Smith, Y. J. Yoon, Y. Chang, Y. Jiang, Z. Lin, Z. V. Vardeny, V. V Tsukruk, *Adv. Opt. Mater.* **2018**, *6*, 1800474.

[193] X. Li, Y. Wang, H. Sun, H. Zeng, *Adv. Mater.* **2017**, *29*, 1701185.

[194] H. Zhu, Y. Fu, F. Meng, X. Wu, Z. Gong, Q. Ding, M. V Gustafsson, M. T. Trinh, S. Jin, X.-Y. Zhu, *Nat. Mater.* **2015**, *14*, 636.

[195] Y. Fu, H. Zhu, C. C. Stoumpos, Q. Ding, J. Wang, M. G. Kanatzidis, X. Zhu, S. Jin, *ACS Nano* **2016**, *10*, 7963.

[196] S. W. Eaton, M. Lai, N. A. Gibson, A. B. Wong, L. Dou, J. Ma, L.-W. Wang, S. R. Leone, P. Yang, *Proc. Natl. Acad. Sci. U. S. A.* **2016**, *113*, 1993.

[197] K. Park, J. W. Lee, J. D. Kim, N. S. Han, D. M. Jang, S. Jeong, J. Park, J. K. Song, *J. Phys. Chem. Lett.* **2016**, *7*, 3703.

[198] H. Zhou, S. Yuan, X. Wang, T. Xu, X. Wang, H. Li, W. Zheng, P. Fan, Y. Li, L. Sun,

A. Pan, *ACS Nano* **2017**, *11*, 1189.

[199] T. J. S. Evans, A. Schlaus, Y. Fu, X. Zhong, T. L. Atallah, M. S. Spencer, L. E. Brus, S. Jin, X.-Y. Zhu, *Adv. Opt. Mater.* **2018**, *6*, 1700982.

[200] Q. Liao, K. Hu, H. Zhang, X. Wang, J. Yao, H. Fu, *Adv. Mater.* **2015**, *27*, 3405.

[201] Q. Zhang, R. Su, X. Liu, J. Xing, T. C. Sum, Q. Xiong, *Adv. Funct. Mater.* **2016**, *26*, 6238.

[202] H. Liu, Z. Wu, J. Shao, D. Yao, H. Gao, Y. Liu, W. Yu, H. Zhang, B. Yang, *ACS Nano* **2017**, *11*, 2239.

[203] R. Dong, Y. Fang, J. Chae, J. Dai, Z. Xiao, Q. Dong, Y. Yuan, A. Centrone, X. C. Zeng, J. Huang, *Adv. Mater.* **2015**, *27*, 1912.

[204] T. Qiu, Y. Hu, F. Xu, Z. Yan, F. Bai, G. Jia, S. Zhang, *Nanoscale* **2018**, *10*, 20963.

[205] J. Song, L. Xu, J. Li, J. Xue, Y. Dong, X. Li, H. Zeng, *Adv. Mater.* **2016**, *28*, 4861.

[206] H. Chen, H. Liu, Z. Zhang, K. Hu, X. Fang, *Adv. Mater.* **2016**, *28*, 403.

[207] L. Dou, Y. (Micheal) Yang, J. You, Z. Hong, W.-H. Chang, G. Li, Y. Yang, *Nat. Commun.* **2014**, *5*, 5404.

[208] F.-X. Liang, J.-Z. Wang, Z.-X. Zhang, Y.-Y. Wang, Y. Gao, L.-B. Luo, *Adv. Opt. Mater.* **2017**, *5*, 1700654.

[209] P. Ramasamy, D.-H. Lim, B. Kim, S.-H. Lee, M.-S. Lee, J.-S. Lee, *Chem. Commun.* **2016**, *52*, 2067.

[210] X. Li, D. Yu, J. Chen, Y. Wang, F. Cao, Y. Wei, Y. Wu, L. Wang, Y. Zhu, Z. Sun, J. Ji, Y. Shen, H. Sun, H. Zeng, *ACS Nano* **2017**, *11*, 2015.

[211] H.-C. Cheng, G. Wang, D. Li, Q. He, A. Yin, Y. Liu, H. Wu, M. Ding, Y. Huang, X. Duan, *Nano Lett.* **2016**, *16*, 367.

[212] R. L. Penn, J. F. Banfield, *Science* **1998**, *281*, 969.

[213] E. Horváth, M. Spina, Z. Szekrényes, K. Kamarás, R. Gaal, D. Gachet, L. Forró, *Nano Lett.* **2014**, *14*, 6761.

[214] H. Deng, D. Dong, K. Qiao, L. Bu, B. Li, D. Yang, H.-E. Wang, Y. Cheng, Z. Zhao, J. Tang, H. Song, *Nanoscale* **2015**, *7*, 4163.

[215] M. Shoaib, X. Zhang, X. Wang, H. Zhou, T. Xu, X. Wang, X. Hu, H. Liu, X. Fan, W. Zheng, T. Yang, S. Yang, Q. Zhang, X. Zhu, L. Sun, A. Pan, *J. Am. Chem. Soc.* **2017**, *139*, 15592.

[216] T. Yang, Y. Zheng, Z. Du, W. Liu, Z. Yang, F. Gao, L. Wang, K.-C. Chou, X. Hou, W. Yang, *ACS Nano* **2018**, *12*, 1611.

[217] B. Yang, F. Zhang, J. Chen, S. Yang, X. Xia, T. Pullerits, W. Deng, K. Han, *Adv. Mater.* **2017**, *29*, 1703758.

[218] Z. Lian, Q. Yan, Q. Lv, Y. Wang, L. Liu, L. Zhang, S. Pan, Q. Li, L. Wang, J.-L. Sun, *Sci. Rep.* **2015**, *5*, 16563.

[219] M. Chen, M.-G. Ju, H. F. Garces, A. D. Carl, L. K. Ono, Z. Hawash, Y. Zhang, T. Shen, Y. Qi, R. L. Grimm, D. Pacifici, X. C. Zeng, Y. Zhou, N. P. Padture, *Nat. Commun.* **2019**, *10*, 16.

[220] X. Li, M. Ibrahim Dar, C. Yi, J. Luo, M. Tschumi, S. M. Zakeeruddin, M. K. Nazeeruddin, H. Han, M. Grätzel, *Nat. Chem.* **2015**, *7*, 703.

[221] F. Palazon, Q. A. Akkerman, M. Prato, L. Manna, *ACS Nano* **2016**, *10*, 1224.

[222] X. Li, D. Yu, F. Cao, Y. Gu, Y. Wei, Y. Wu, J. Song, H. Zeng, *Adv. Funct. Mater.* **2016**, *26*, 5903.

[223] A. Swarnkar, V. K. Ravi, A. Nag, *ACS Energy Lett.* **2017**, *2*, 1089.

[224] D. E. Scaife, P. F. Weller, W. G. Fisher, *J. Solid State Chem.* **1974**, *9*, 308.

[225] X. Qiu, B. Cao, S. Yuan, X. Chen, Z. Qiu, Y. Jiang, Q. Ye, H. Wang, H. Zeng, J. Liu, M. G. Kanatzidis, *Sol. Energy Mater. Sol. Cells* **2017**, *159*, 227.

[226] B. Pradhan, G. S. Kumar, S. Sain, A. Dalui, U. K. Ghorai, S. K. Pradhan, S. Acharya, *Chem. Mater.* **2018**, *30*, 2135.

[227] M. Zhang, H. Yu, M. Lyu, Q. Wang, J.-H. Yun, L. Wang, *Chem. Commun.* **2014**, *50*,

11727.

[228] S. Gonzalez-Carrero, R. E. Galian, J. Pérez-Prieto, *Opt. Express* **2016**, *24*, A285.

[229] C. Wehrenfennig, M. Liu, H. J. Snaith, M. B. Johnston, L. M. Herz, *J. Phys. Chem. Lett.* **2014**, *5*, 1300.

[230] D. Nguyen Minh, J. Kim, J. Hyon, J. Hyun Sim, H. H. Sowlih, C. Seo, J. Nam, S. Eom, S. Suk, S. Lee, E. Kim, Y. Kang, *Chem. Mater* **2017**, *29*, 5713.

[231] I. Levchuk, A. Osvet, X. Tang, M. Brandl, J. D. Perea, F. Hoegl, G. J. Matt, R. Hock, M. Batentschuk, C. J. Brabec, *Nano Lett* **2017**, *17*, 2765.

[232] L. Zhou, J.-F. Liao, Z.-G. Huang, X.-D. Wang, Y.-F. Xu, H.-Y. Chen, D.-B. Kuang, C.-Y. Su, *ACS Energy Lett.* **2018**, *3*, 2613.

[233] S. Kumar, J. Jagielski, S. Yakunin, P. Rice, Y.-C. Chiu, M. Wang, G. Nedelcu, Y. Kim, S. Lin, E. J. G. Santos, M. V. Kovalenko, C.-J. Shih, *ACS Nano* **2016**, *10*, 9720.

[234] H. Huang, F. Zhao, L. Liu, F. Zhang, X. Wu, L. Shi, B. Zou, Q. Pei, H. Zhong, *ACS Appl. Mater. Interfaces* **2015**, *7*, 28128.

[235] W. Deng, X. Xu, X. Zhang, Y. Zhang, X. Jin, L. Wang, S.-T. Lee, J. Jie, *Adv. Funct. Mater.* **2016**, *26*, 4797.

[236] M. F. Aygüler, M. D. Weber, B. M. D. Puscher, D. D. Medina, P. Docampo, R. D. Costa, *J. Phys. Chem. C* **2015**, *119*, 12047.

[237] M. Yuan, L. N. Quan, R. Comin, G. Walters, R. Sabatini, O. Voznyy, S. Hoogland, Y. Zhao, E. M. Beauregard, P. Kanjanaboos, Z. Lu, D. H. Kim, E. H. Sargent, *Nat. Nanotechnol.* **2016**, *11*, 872.

[238] T. Chiba, K. Hoshi, Y.-J. Pu, Y. Takeda, Y. Hayashi, S. Ohisa, S. Kawata, J. Kido, *ACS Appl. Mater. Interfaces* **2017**, *9*, 18054.

[239] X. Zhang, B. Xu, J. Zhang, Y. Gao, Y. Zheng, K. Wang, X. W. Sun, *Adv. Funct. Mater.* **2016**, *26*, 4595.

[240] X. Zhang, C. Sun, Y. Zhang, H. Wu, C. Ji, Y. Chuai, P. Wang, S. Wen, C. Zhang, W.

W. Yu, *J. Phys. Chem. Lett.* **2016**, *7*, 4602.

[241] J. Pan, L. N. Quan, Y. Zhao, W. Peng, B. Murali, S. P. Sarmah, M. Yuan, L. Sinatra, N. M. Alyami, J. Liu, E. Yassitepe, Z. Yang, O. Voznyy, R. Comin, M. N. Hedhili, O. F. Mohammed, Z. H. Lu, D. H. Kim, E. H. Sargent, O. M. Bakr, *Adv. Mater.* **2016**, *28*, 8718.

[242] J. B. Hoffman, G. Zaiats, I. Wappes, P. V. Kamat, *Chem. Mater.* **2017**, *29*, 9767.

[243] A. Hazarika, Q. Zhao, E. A. Gaulding, J. A. Christians, B. Dou, A. R. Marshall, T. Moot, J. J. Berry, J. C. Johnson, J. M. Luther, *ACS Nano* **2018**, *12*, 10327.

[244] Z. Yang, J. Z. Fan, A. H. Proppe, F. P. G. de Arquer, D. Rossouw, O. Voznyy, X. Lan, M. Liu, G. Walters, R. Quintero-Bermudez, B. Sun, S. Hoogland, G. A. Botton, S. O. Kelley, E. H. Sargent, *Nat. Commun.* **2017**, *8*, 1325.

[245] Q. A. Akkerman, M. Gandini, F. Di Stasio, P. Rastogi, F. Palazon, G. Bertoni, J. M. Ball, M. Prato, A. Petrozza, L. Manna, *Nat. Energy* **2017**, *2*, 16194.

[246] X. Zhang, Z. Jin, J. Zhang, D. Bai, H. Bian, K. Wang, J. Sun, Q. Wang, S. F. Liu, *ACS Appl. Mater. Interfaces* **2018**, *10*, 7145.

[247] X. Zhang, Q. Wang, Z. Jin, J. Zhang, S. (Frank) Liu, *Nanoscale* **2017**, *9*, 6278.

[248] H. Wu, H. Si, Z. Zhang, Z. Kang, P. Wu, L. Zhou, S. Zhang, Z. Zhang, Q. Liao, Y. Zhang, *Adv. Sci.* **2018**, *5*, 1801219.

[249] M. Gong, R. Sakidja, R. Goul, D. Ewing, M. Casper, A. Stramel, A. Elliot, J. Z. Wu, *ACS Nano* **2019**, *13*, 1772.

Figures

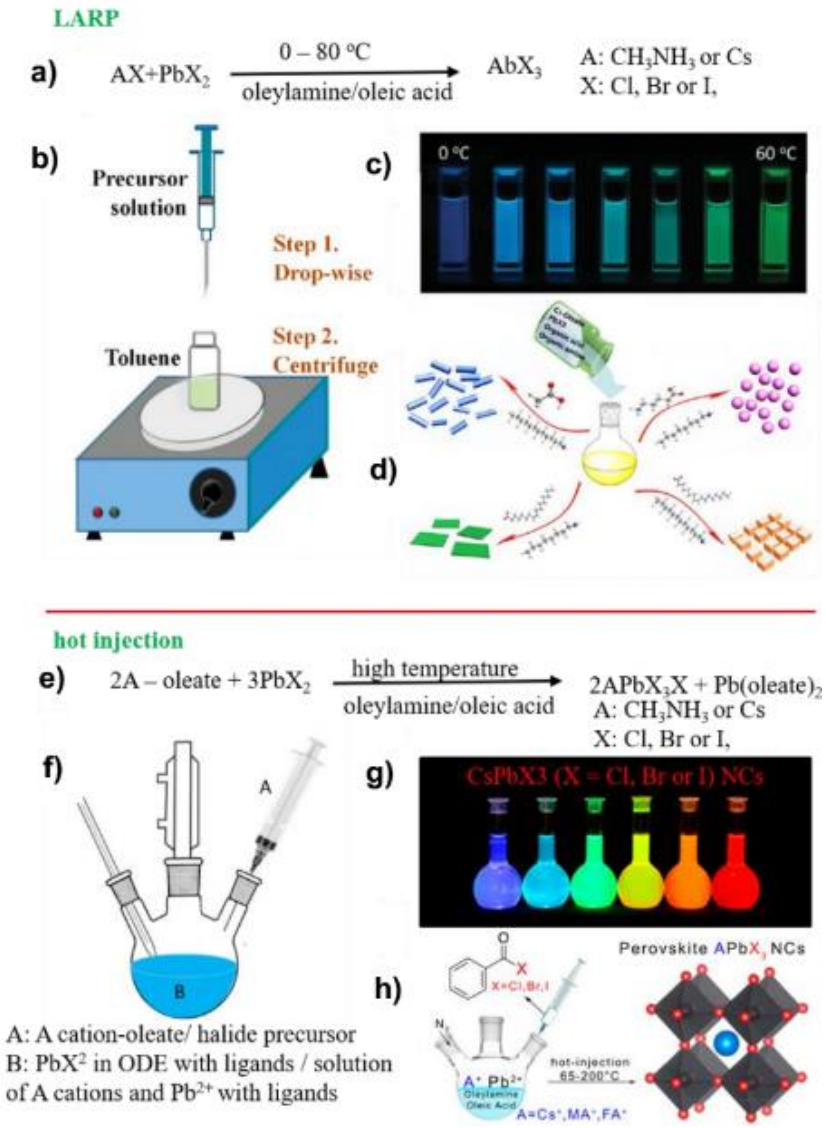

Figure 1. (a) LARP synthesis of PNCs. (b) Schematic diagram of LARP reaction system. Reproduced with permission.[36] (c) Photographs of colloidal solution of $MAPbBr_3$ NCs obtained by using different temperature of toluene solution. Reproduced with permission.[49] (d) Different shaped $CsPbX_3$ NCs synthesized by LARP method. Reproduced with permission.[44] (e) Hot injection synthesis of PNCs. (f) Schematic diagram of hot injection system. Reproduced with permission.[47] (g) Photograph of colloidal solution of $MAPbX_3$ (X = Cl, Br or I) NCs. Reproduced with permission.[35] (h) Hot injection synthesis of PNCs using benzoyl halides as halide precursors. Reproduced with permission.[54]

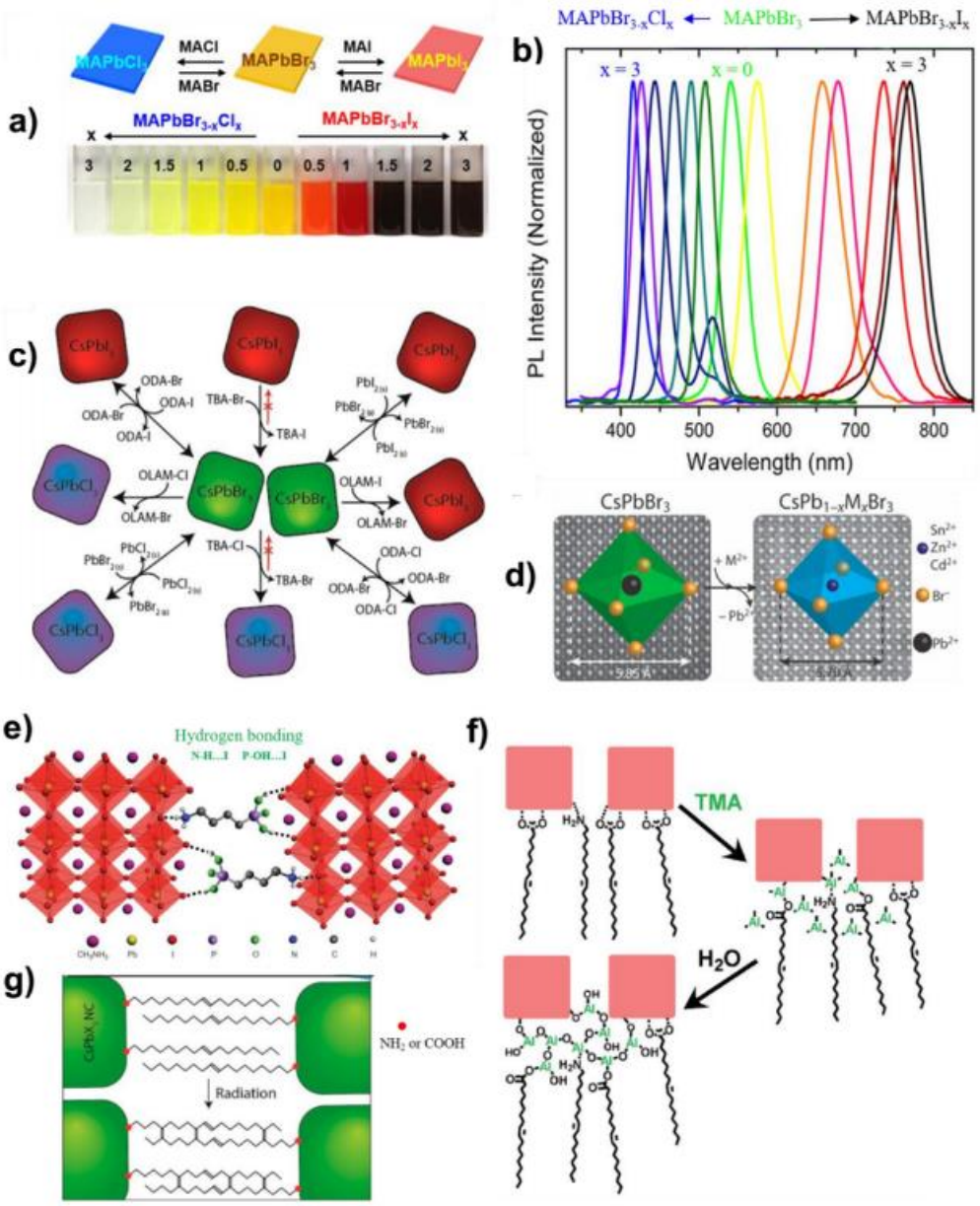

Figure 2. (a) Photograph of halide anion-exchanged, mixed-halide $MAPbBr_{3-x}Cl_x$ and $MAPbBr_{3-x}I_x$ NC under room light. (b) PL spectra of $MAPbBr_{3-x}Cl_x$ and $MAPbBr_{3-x}I_x$ NCs. Reproduced with permission.[56] (c) Different routes and precursors for $CsPbX_3$ (X = Cl, Br, I) halide anion exchange. Reproduced with permission.[57] (d) Schematic illustration of the replacement of B site in cubic PNCs. Reproduced with permission.[64] (e) Schematic illustration of interconnection of two neighboring grain structures by additives. Reproduced with permission.[220] (f) Reaction schematic of the TMA crosslinking process. Reproduced with permission.[160] (g) Schematic representation of the irradiation induced graphitization process. Reproduced with permission.[221]

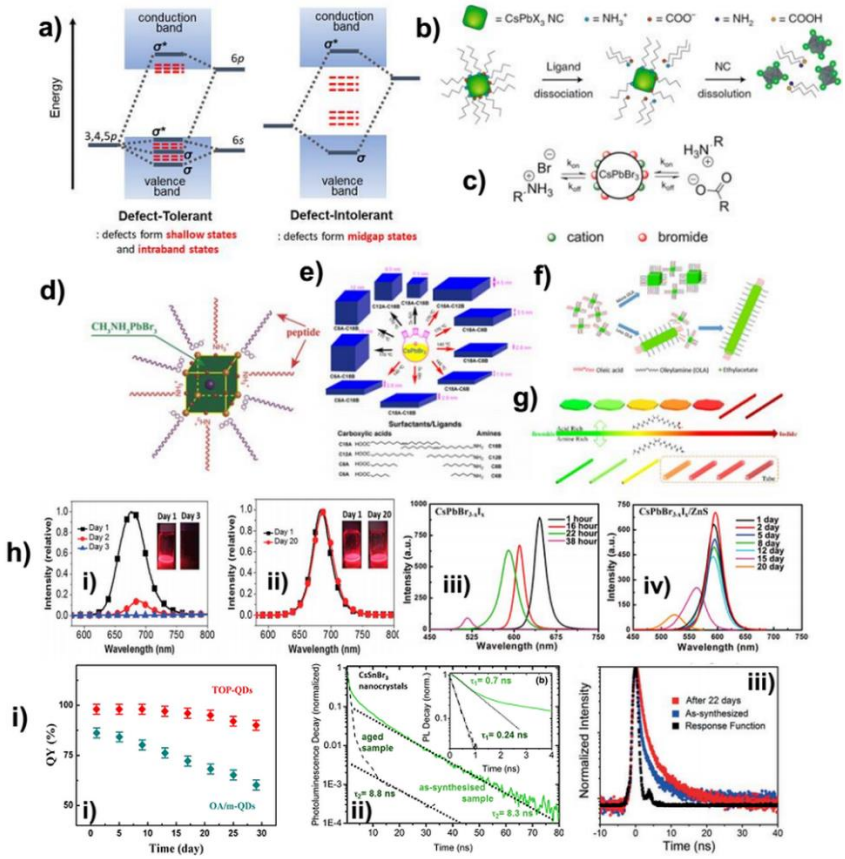

Figure 3. (a) Energy structure of perovskite nanocrystals yielding the unique defect-tolerant electronic and optical properties in comparison to that of conventional defect-intolerant semiconductors. Reproduced with permission.[29] (b) Structure lability of $CsPbX_3$ NCs due to the desorption of weakly bound ligands. Reproduced with permission.[48] (c) Schematic diagram illustrating the dynamic surface stabilization of $CsPbBr_3$ NCs by oleylammonium bromide. Reproduced with permission.[100] (d) Schematic diagram illustrating the surface passivation of mechanism of Br and Pb surface defects. Reproduced with permission.[101] (e) Morphology of $CsPbBr_3$ NCs as a function of reaction temperature and identity of surface ligands. Reproduced with permission.[53] (f) Schematic diagram illustrating that different ration of OLA can control the shape of the NCs. Reproduced with permission.[106] (g) Schematic illustration for the formation of perovskite nanowires and nanosheets NCs. Reproduced with permission.[107] (h) PL spectra for $CsPbI_3$−OA (i) and $CsPbI_3$−TMPPA (ii). Insets of (i and ii): Solutions of the respective washed NCs under UV light at different times following synthesis. Reproduced with permission.[102] Optical stability of (iii) $CsPbBr_{3-x}I_x$ and (iv) $CsPbBr_{3-x}I_x$/ZnS. Reproduced with permission.[123] (i) (i) Change of the PL QY of the OA/m−,TOP−$CsPbI_3$ QDs versus storage time, where QD solutions synthesized at 140°C were stored in a sealed bottle under ambient conditions. Reproduced with permission.[124] (ii) Fast (inset) and slow PL decay kinetics of as-synthesized and aged $CsSnBr_3$ nanocrystals in solution, excited at 490 nm, and detected at 590−900 nm. Reproduced with permission.[125] (iii) TR-PL kinetics of as-synthesized ligand-free $Cs_3Bi_2Br_9$ NCs and after being stored in open air for 22 days. Reproduced with permission.[69]

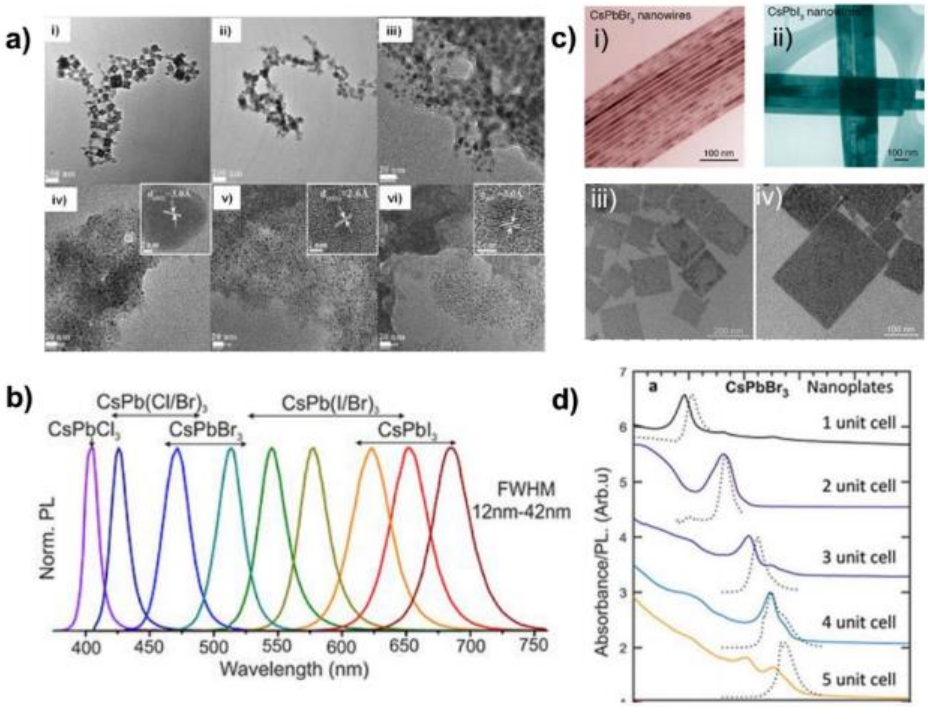

Figure 4. (a) TEM images of PNCs prepared with different concentrations of APTES capping ligands: i) $PNC_{APTES-2}$, ii) $PNC_{APTES-4}$, iii) $PNC_{APTES-8}$, iv) $PNC_{APTES-16}$, v) $PNC_{APTES-32}$, and vi) $PNC_{APTES-64}$. (b) Colloidal perovskite $CsPbX_3$ NCs (X = Cl, Br, I) exhibit size- and composition-tunable bandgap energies covering the entire visible spectral region with narrow and bright emission: representative PL spectra (λ_{ex}= 400 nm for all but 350 nm for $CsPbCl_3$ samples). Reproduced with permission.[35] (c) Colorful SEM images of as-prepared (i) $CsPbBr_3$ and (ii) $CsPbI_3$ nanostructures grown from solution. Reproduced with permission.[130] (iii, iv) TEM images of $CsPbClBr_2$ and $CsPbBr_2I$ mixed perovskite nanosheets, respectively. Reproduced with permission.[145] (d) Absorption and photoluminescence spectra of $CsPbBr_3$ nanoplatelets of different thicknesses (n =1, 2, 3, 4, 5, and ∞) prepared by lowering the temperature during the hot injection synthesis method. Reproduced with permission.[132]

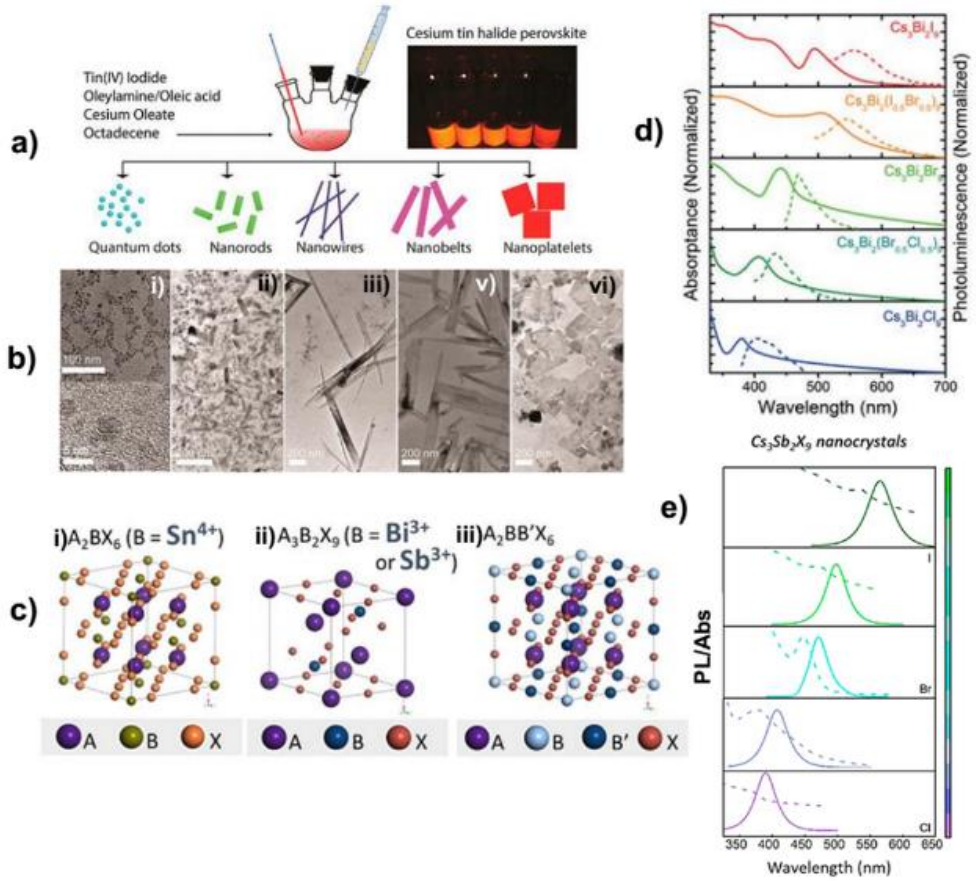

Figure 5. (a) Synthesis of Cs_2SnI_6 nanocrystals: schematic diagram of procedures for the controlled synthesis of perovskite Cs_2SnI_6 nanocrystals (left panel) and photograph of the as-prepared Cs_2SnI_6 samples under UV light (right panel). (b) TEM images of Cs_2SnI_6 nanocrystals (i-vi) with different shapes (the inset of (i) gives an HRTEM image of Cs_2SnI_6 spherical quantum dots). Reproduced with permission.[135] (c) Schematic of i) AB_2X_6, ii) $A_3B_2X_9$, iii) $A_2BB'X_6$ perovskite structures.[18,125,136]. (d) Steady-state absorption and PL spectra of $Cs_3Bi_2X_9$ NCs containing pure and mixed halides. Reproduced with permission.[69] (e) Tunable PL spectra for $Cs_3Sb_2X_9$ ($X = Cl_xBr_yI_{1-x-y}, 0 \leq x, y \leq 1$) nanocrystals prepared by the anion exchange from $Cs_3Sb_2Br_9$ nanocrystals. Reproduced with permission.[91]

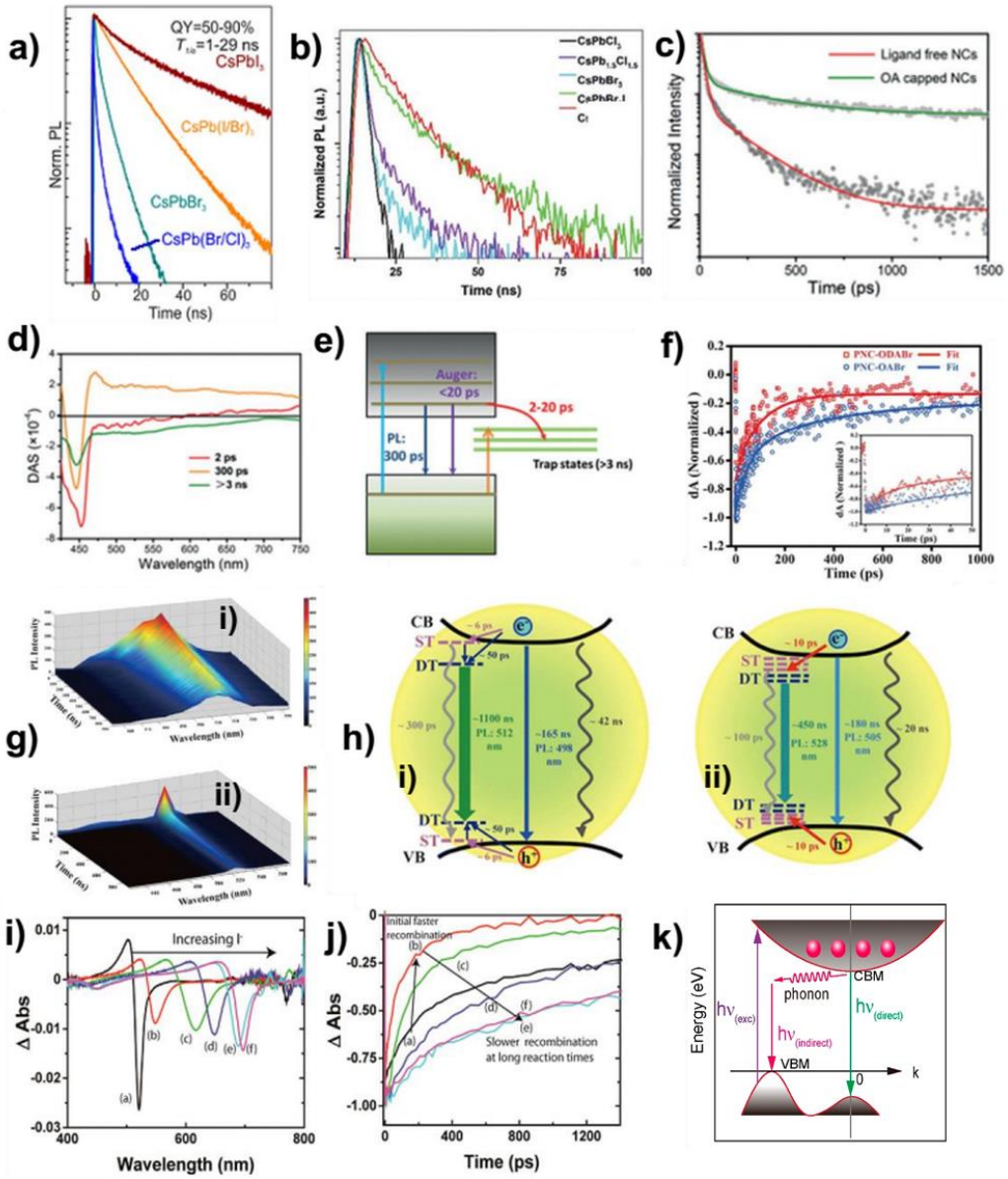

Figure 6. (a) Time-resolved PL decays for $CsPbX_3$ (X=Cl, Br, I) nanocrystals by the dependence of halide composition. Reproduced with permission.[35] (b) Time-dependent PL decays of various $CsPbX_3$ nanosheets. Reproduced with permission.[145] (c) TR-PL kinetics of ligand-free NCs and OA capped NCs measured with streak camera. (d) DAS for three fitting components from TA spectra. (e) Excited dynamics model of $Cs_3Bi_2Br_9$ NCs. Reproduced with permission.[69] (f) Normalized TA recovery profiles of PNC−OABr and PNC−ODABr with 40 nJ/pulse over 0−1000 ps time delay. (Inset) TA profiles over 0−50 ps time delay. (g) Three-dimensional TRPL spectra of (i) PNC−OABr and (ii) PNC−ODABr, which were collected at 10 nm intervals spanning the width of the PL emission peaks. (h) Schematic illustration of the energy band structure and proposed assignment of lifetimes of various excitonic processes for (i) PNC−OABr and (ii) PNC−ODABr based on the TA and TRPL results. Reproduced with permission.[146] (i) Difference absorption spectra at 10 ps delay for 25 nm thick $CsPbBr_3$ NC films soaked at 120 °C for (a) 0 s, (b) 10 s, (c) 30 s, (d) 1 min, (e) 3 min, (f) 25 min. (j) Kinetic traces recorded at the main bleach maxima for the same films. At short exchange times the bleach kinetics become significantly faster, but slowed as more iodide was introduced. Reproduced with permission.[143] (k) Proposed recombination pathways in $Cs_3Bi_2I_9$. Reproduced with permission.[151]

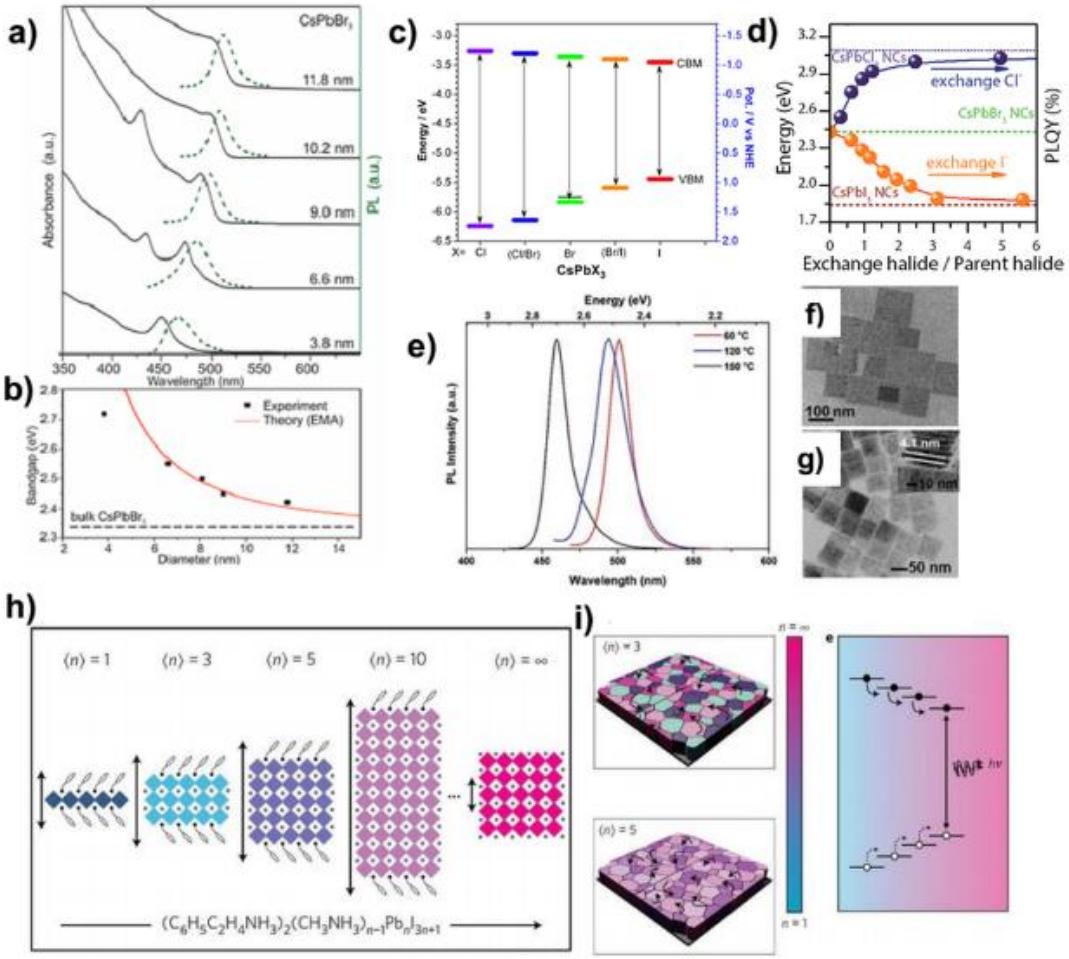

Figure 7. (a) Quantum-size effects in the absorption and emission spectra of 5−12 nm $CsPbBr_3$ NCs. (b) Experimental versus theoretical (effective mass approximation, EMA) size dependence of the band gap energy. Reproduced with permission.[35] (c) Band edge energies of $CsPbX_3$ nanocrystals estimated by cyclic voltammetry. Reproduced with permission.[96] (d) PL calibration curves: a targeted emission energy could be obtained by adding a precise amount of halide precursor to a crude solution of $CsPbBr_3$ NCs. The curves are reported as a function of the molar ratio between the added halide (or exchange halide) and the Br amount in the starting NCs. Reproduced with permission.[57] (e) PL spectra of $CsPbBr_3$ nanosheets synthesized at different temperatures. (f, g) TEM images of 2- and 4-monolayer-thick $CsPbBr_3$ nanosheets synthesized at 150 and 60 °C, respectively. Inset: side view of stacking $CsPbBr_3$ nanosheets synthesized at 60 °C. Reproduced with permission.[145] (h) Perovskite nanostructures with different thicknesses (n =number of layers), showing the evolution of 2D (n =1) to 3D (n = ∞). i) Schematic illustration of carrier transfer in n =3 and n =5 perovskites in a thin film made of mixed (n =1 to ∞) structures and a scheme showing the energy channeling to a lowest band gap emitter. Reproduced with permission.[158]

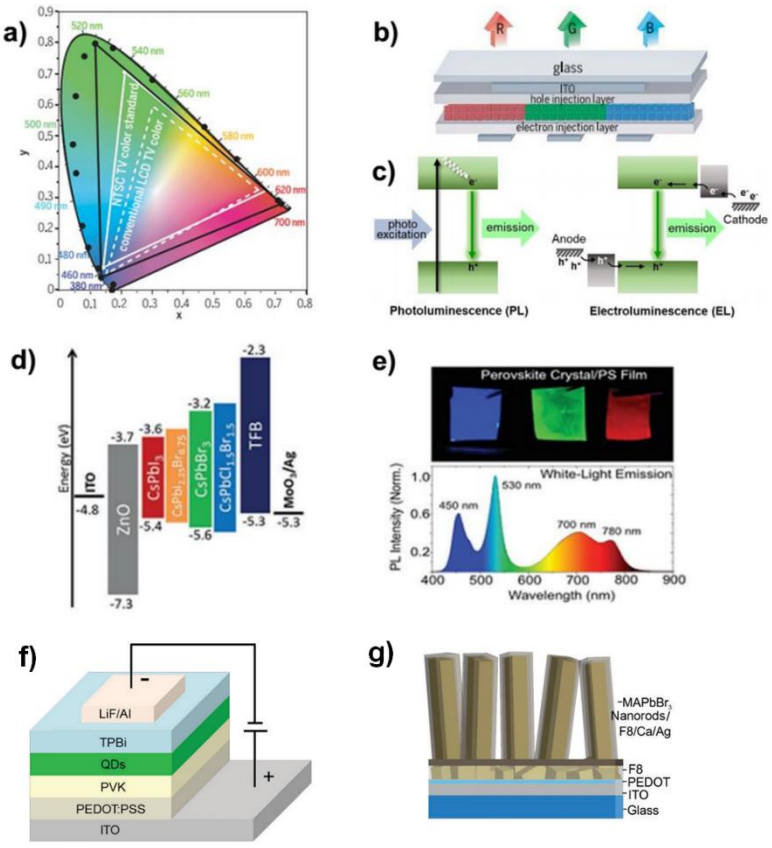

Figure 8. (a) PL spectra of $CsPbX_3$NCs plotted on CIE chromaticity coordinates (black points) compared with common color standards (LCD television, dashed white line, and NTSC television, solid white line), reaching 140% of the NTSC color standard (solid black line). Reproduced with permission.[29] (b) Schematic of a three-color LED pixel with LHP NCs as the emissive layer. Reproduced with permission.[4] (c) Schematic description of electroluminescence and photoluminescence. Reproduced with permission.[78] (d) Energy-level diagram for typical perovskite NC LEDs. Reproduced with permission.[160] (e) Perovskite crystals for tunable white-light emission. Reproduced with permission.[163] (f) A representative device structure of a multilayer perovskite LED based on $CsPbX_3$QDs. Reproduced with permission.[5] (g) Device structure of a $MAPbBr_3$ nanorod array LED. Reproduced with permission.[156]

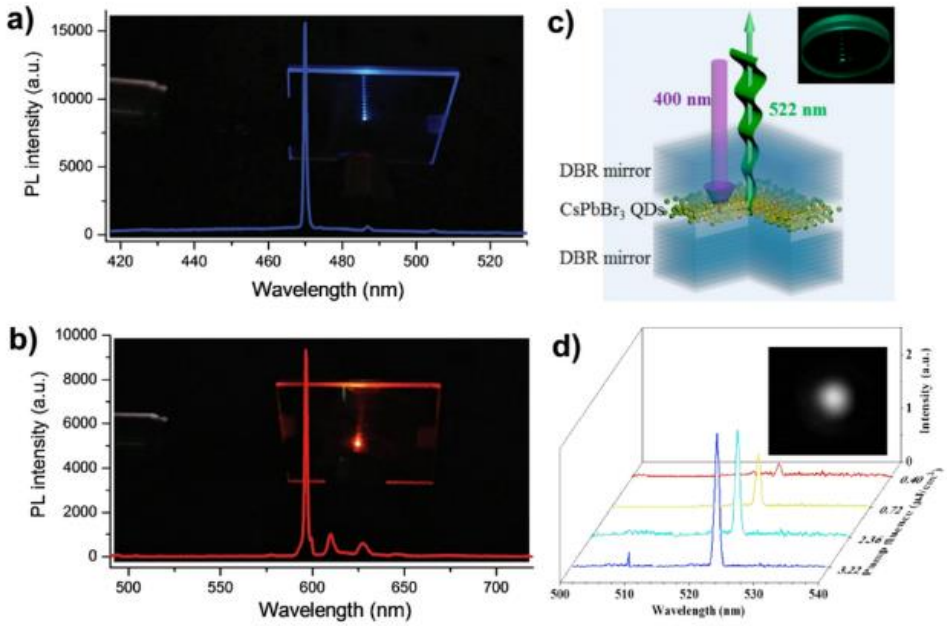

Figure 9. Microcavity based $CsPbX_3$ NC lasers. (a) Schematic of the device structure and a photograph of a $CsPbBr_3$ NC laser under optical pumping. (b) Emission spectrum of the device in (a) above the lasing threshold (0.39 μJ/cm^2) and the far-field emission pattern of the device. Only a single lasing mode is observed. Reproduced with permission.[191] (c) and (d), microcavity lasers based on $CsPb(Br/Cl)_3$ (c) and $CsPb(I/Br)_3$ NCs. Emission spectra measured above the lasing thresholds at 38.2 μJ/cm^2 (1.5 times the threshold intensity) for (c) and at 30.5 μJ/cm^2 (1.6 times the threshold intensity) for (d). Multiple lasing peaks are seen, due to the thicker layer of NC gain material used. Reproduced with permission.[190]

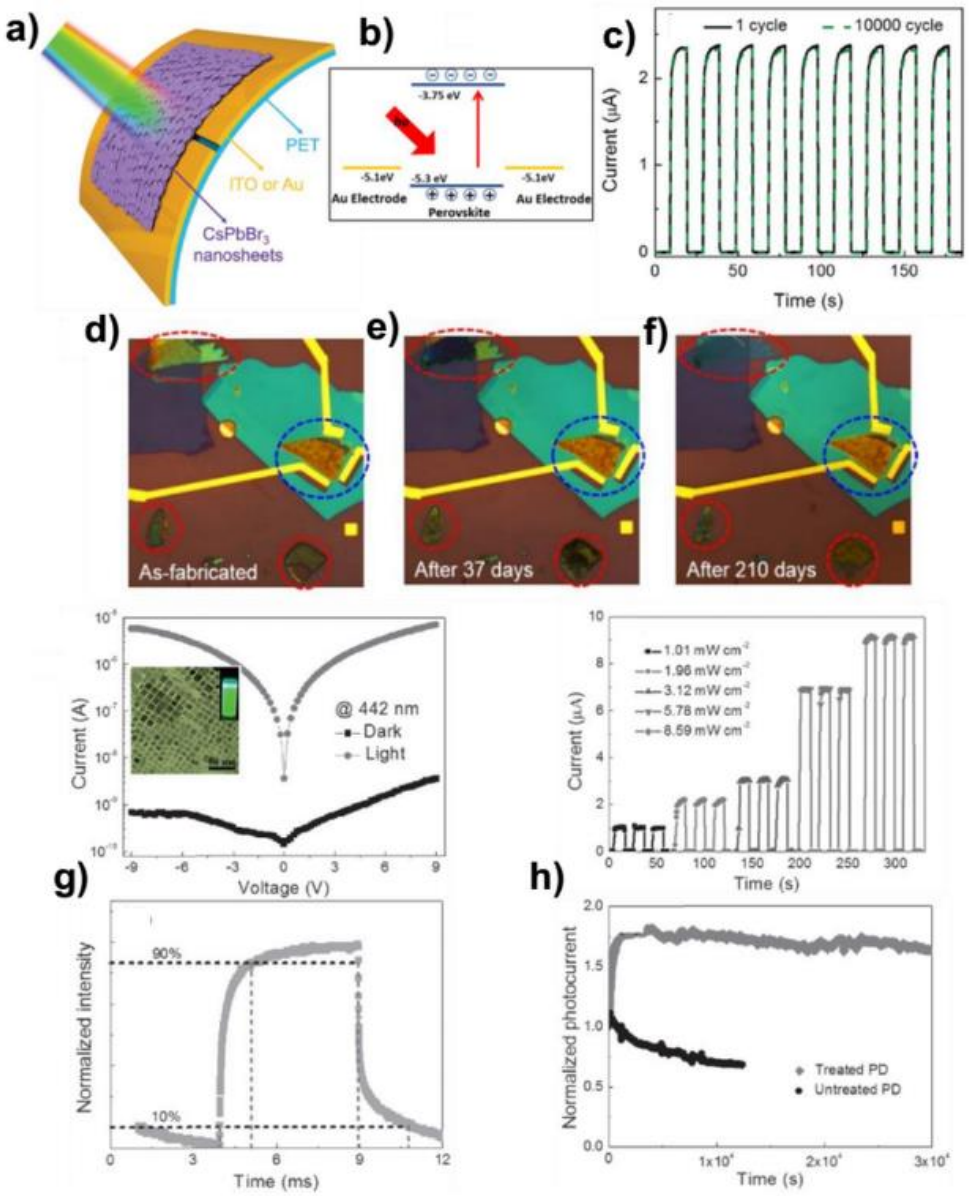

Figure 10. (a) Printed flexible 2D perovskite photodetectors. (b) Schematic representation of a typical perovskite-Au energy band alignment configuration where electron-hole pairs are generated under illumination. Reproduced with permission.[205] (c) Photoresponse at 5V of the $CsPbBr_3$ nanosheet photodetector for the 1st and 10 000th bending-recovery cycle. (d) Optical image of BN-covered photodetector device. The red dashed circles indicate some perovskite flakes that were not covered by BN, while the BN-covered devices are indicated by a blue dashed circle. The 2D perovskite NCs from upper left corner (red dashed cycle) was damaged after 37 days, while the middle BN-protect 2D perovskite NCs (blue dashed cycle) exhibited quite stable even after 210 days. Reproduced with permission.[211] (e) Logarithmic I–V plot of the photodetector (PD) of Au/$CsPbBr_3$/Au on SiO_2 substrate measured in dark and under monochromatic light at the wavelength of 442 and intensity of mW cm^{-2}. The inset figure in (d) represents TEM images of the nanocrystals grown. (f) Photo response of detector at different intensities of constant 3 V bias under 442 nm. Rise and decay time in (g) indicating 1.8 and 1 ms respectively. (h) Illustrates the stability comparison of treated and untreated photodetectors under continuous irradiation for more than 8 h (3 V, 442 nm, 3.12 mW cm^{-2}). Reproduced with permission.[222]

Tables

Table 1. Properties of selected Pb-free PNCs.

PNCs	Synthesis	Crystal structure	Advantages	Disadvantages	Ref.
$CsSnX_3$ (X= Br, Cl, I)	Hot injection or anion exchange	Cubic (Cl), orthorhombic (Br,I)	High hole mobility; Tunable bandgap through Vis/NIR	High sensitivity to moisture, oxygen, thermal treatments; PLQY<1%	[79,125,223,224]
Cs_2SnI_6	Phosphine-free hot injection	Defect-variant of ABX_3 perovskite structure	Stable films; direct bandgap (1.48 eV); high absorption coefficient; tunable morphology; tested in solar cells and FETs	Material degradation upon applied voltage is poor (*e.g.* in solar cells)	[135,225]
$Cs_3Bi_2X_9$ (X= Br, Cl, I)	Hot injection[84] or room T synthesis[69]	Vacancy-ordered ABX_3 perovskite structure	Widely-tunable absorbance; air stable	Origin of the observed PL unclear; low electronic dimensionality	[69,84]
$MA_3Bi_2X_9$ (X=Cl, Br, I)	Collaborative solvent LARP (Co-LARP)	Distorted-layered structure	PLQY=15% (X=Br); tunable PL peaks from 360 to 540 nm; good ethanolic stability; minor re-absorption effect	PLQY=0.03% (X=I)	[83]
$Cs_3Sb_2X_9$ (X=Cl, I)	Ionic metathesis process (X=Cl)	Trigonal and orthorhombic phases	Band-edge emission in the yellow-red (X=I); Sharp band-edge excitonic emission	Better control of defect chemistry is needed	[137,226]
Cs_2AgBiX_6 (X=Cl, Br, I)	Hot injection (X=Cl, Br), anion exchange reaction (X=I)	Elpasolite (X=Cl, Br)	Stable, strong absorption throughout the visible region	Indirect bandgap	[68]
$Cs_2InSbCl_6$	--	--	Direct bandgap (1.0 eV); stable	Not yet synthesized	[18]
$Cs_2AgIn_xBi_{1-x}Cl_6$ (x = 0.75 and 0.9)	Anti-solvent recrystallization	Fm3m cubic space group	Direct bandgap; PLQY=36.6%; bright dual color (violet and orange) emission	Not yet tested in any device	[67]

Table 2. Quantum yields (QY), average PL decay lifetimes (τ_{avg}), radiative recombination lifetimes (τ_r), and nonradiative recombination lifetimes (τ_{nr}) of various perovskite nanocrystals.

PNCs	Dimensionality	PLQY [%]	τ_{avg} [ns]	τ_r [ns]	τ_{nr} [ns]	Ref.
$MAPbBr_3$	0 D	50-70	13.5	6.6	18	[36]
		74-93	13-27	14-36	101-252	[49]
$MAPbBr_{3-x}Cl_x$	0 D	20-83	100-446	49-430	180-480	[227][228]
$MAPbI_{3-x}Cl_x$	0 D	13-75	44	38	95	[227][228]
$MAPbI_3$	0 D/1 D/2 D	2-55	100	94	180	[229][105]
$FA_xMA_{1-x}PbI_3$	1 D	N/A	490-1940	350-1010	590-2850	[155]
$FAPbX_3$	0 D/1 D	1-85	15-264	7.8-32	58-290	[155][230][231]
$CsPbX_3$	2 D	1-23	3.5-18	2-20	23-70	[145]
(X=Cl, Br, I)	0 D/1 D	50-90	1-29	0.5-25	8-65	[35]
$CsPbI_3$	0 D	~100	36	31	140	[124]
$CsSnX_3$ (X=Cl, Br, I)	3 D	< 1	2.5-10.3	0.3-4.1	2.7-12.3	[125]
Cs_2SnCl_6:Bi	3 D	~80	343	290	560	[156]
Cs_2PdBr_6	2 D	0.3	0.9	0.5	4.2	[232]
$Cs_3Bi_2Br_9$	0 D	0.2-4.5	34-51	10-15	40-60	[69]

Table 3. Summary of the performance of PNCs-based LEDs.

PNCs	Morphology	EL	EQE_{max} [%]	Current efficiency [cd A^{-1}]	Peak luminance [cd m^{-2}]	FWHM [nm]	Ref.
$MAPbBr_3$	nanoplatelets	blue to green	2.31	8.1	8.5	~30	[233]
	QDs	green	1.1	4.5	2,503	~26	[234]
	nanoparticles	green	8.53	42.9	-	23	[6]
$MAPbBr_{3-x}I_x$	nanorods	orange to black	-	-	-	39-51	[59]
$MAPbX_3$ (X = Cl, Br, I)	QDs	white	1.38	4.01	2,673	21	[235]
$(FA)_{1-x}(MA)_xPbBr_3$	nanoparticles	yellowish green	-	0.013	2	~20	[236]
$PEA_2(MA)_{n-1}Pb_nI_{3n+1}$	nanoplatelets	green to black	8.8	-	-	~50	[237]
$CsPbBr_3$	nanocubes	green	0.06	0.19	1,377	18	[161]
	nanocubes	green	8.73	18.8	100	19	[238]
$CsPbBr_3$-$CsPb_2Br_5$	nanoparticles	green	2.21	8.98	3,853	24	[239]
$CsPbBr_{3-x}I_x$	nanoplatelets and nanocubes	white	-	-	114	25-50	[113]
	nanoparticles	green to red	6.3-7.25	3.4	3019	14-36	[240]
$CsPbBr_xCl_{3-x}$	nanocubes	blue-green (cyan)	3.0	-	330	20	[241]
$CsPbX_3$ (X = Cl, Br, I)	QDs	green	0.12	946	0.43	25	[5]
	nanocubes	blue to red	5.7	-	2,335	17-31	[160]
$CsPb_{0.73}Mn_{0.27}Cl_3$	QDs	orange to red	-	2.2	-	55	[202]
$Cs_3Bi_2Br_9$	QDs	blue	-	-	-	48	[136]

Table 4. Summary of the performance of PNCs-based solar cells.

Active material	Solar cell structure	V_{OC} [V]	J_{SC} [mA/cm^2]	FF [%]	PCE [%]	Ref.
$CsPbBr_3$ QD	FTO|$cTiO_2$|$CsPbBr_3$|Spiro-OMeTAD|Au	1.41	7.05	55	5.5	[242]
$Cs_{1-x}FA_xPbI_3$ NC	FTO|$cTiO_2$|$CsPbI_3$|Spiro-OMeTAD|MoO_x|Al	1.17	15.2	66	11.75	[243]
$FAPbI_3$ (5%) in pDPP5T:PCBM	ITO|ZnO|$Ba(OH)_2$|$FAPbI_3$ (5%) : pDPP5T:PCBM|MoO_x|Ag	0.56	15.22	65.41	5.51	[179]
FAI coated $CsPbI_3$ QD	FTO|$cTiO_2$|$CsPbI_3$-FAI|Spiro-OMeTAD|MoO_x|Al	1.20	14.37	78	13.4	[177]
PVP treated $CH_3NH_3PbCl_xI_{3-x}$	ITO|PEDOT:PSS|$MAPbI_{3-x}Cl_x$:PVP|CYTOP^{TM}|PCBM|PEIE|Ag or Au	0.94	10.50	79	7.91	[181]
$CsPbI_3$	FTO|$cTiO_2$|$CsPbI_3$|Spiro-OMeTAD|MoO_3|Al	~1.2	~15	--	~12	[183]
MaPbI3-PbS:TG-PbS	ITO|ZnO NPs|mixed-QD ink|PbS|Au	0.62	26.8	63.9	10.45	[244]
$CsPbBr_3$	FTO|$cTiO_2$|$CsPbBr_3$|Spiro-OMeTAD|Au	1.5	5.6	62	5.4	[245]
µG/$CsPbI_3$	FTO|$cTiO_2$|µG:$CsPbI_3$|PTAA|Au	1.18	13.59	72.6	11.40	[182]
$CsPbBrI_2$ 3D-2D-0D	FTO|TiO_2|$CsPbBrI_2$ 3D-2D-0D|PTAA|Au	1.19	12.93	80.5	12.39	[180]
$CsPbI_3$	FTO|TiO_2|$CsPbI_3$|Spiro-OMeTAD|MoO_x|Al	1.23	13.47	65	10.77	[175]
$CsPbBr_3$-$CsPb_2Br_5$	FTO|ZnO NP|$CsPbBr_3$-$CsPb_2Br_5$|Spiro-OMeTAD|Au	1.43	6.17	77.2	6.81	[246]
$FAPbI_3$	ITO|SnO_2|$FAPbI_3$|Spiro-OMeTAD|Au	1.10	11.83	64.42	8.38	[184]
$CsPbI_3$	FTO|TiO_2|$CsPbI_2Br$|$CsPbI_3$|PTAA|Au	1.177	80.2	14.25	13.45	[178]
$CsPbI_3$	FTO|TiO_2|$CsPbI_3$|PTB7|MoO_3|Ag	1.27	12.39	11.90	12.55	[185]

Table 5. Summary of the performance of PNCs-based photodetectors.

Device architecture	Method	Input light intensity & wavelength	Bias voltage	Responsivity (A/W)	On/Off ratio	Rise/Decay time	Ref.
Au/$CsPbI_3$/Au	Ion exchange reactions based NCs	1.98 mW/cm^2, 405 nm	1 V	--	10^5	24/29 ms	[209]
Au/α-$CsPbI_3$/Au,	Upconverion (NaYF4:Yb,Er QDs) surface-modified	10 mW/cm^2, 525 nm	5 V	1.5	10^4	5/5 ms	[247]
ITO/$CsPbBr_3$/ITO	Nanosheets from chemical routes	0.35 mW/cm^2, 442 nm	5 V	0.64	10^4	0.019/0.024 ms	[205]
Graphene/$MAPbI_3$/Graphene	2D $MAPbI_3$ based on vapor-phase intercalation	532 nm	1 V	950	10^6	22/27 ms	[211]
Au/$CsPbI_{3-x}Br_x$/MoS_2/Au	Chemical route based QDs	532 nm	0.1 V	7.7×10^4	10^4	590/320	[248]
Au/$CsPbBr_3$/Au	Centrifugal casting-based NC films	1.01 mW/cm^2, 442 nm	3 V	0.18	8×10^3	1.8/1.0 ms	[222]
Au/$CsPbCl_3$--graphen/Au	multiple process based NCs	8.17 μW/cm^2, 400 nm	0.5 V	10^6	--	0.3/0.35 s	[249]
$CsPbBr_3$/CNTs	Nanosheets from chemical routes	400 nm	10 V	31.1	10^5	0.016/0.38 ms	[210]

Table 6. Comparison between the photophysical properties of perovskite nanocrystals and bulk films.

Photophysical properties	Bulk films	PNCs
optical spectrum	not tunable	tunable
PLQY	low	high
exciton lifetime	long	long
charge-carrier extraction	efficient	limited
charge transfer	fast	limited
charge diffusion length	long	short
charge recombination dynamics	slow	fast

Author biographies and photographs (up to 3 authors)

Maning Liu

Maning Liu received his Ph.D. degree (2017) in Physical Chemistry from Royal Melbourne Institute of Technology (RMIT), Australia. He worked as a senior process engineer for 7 years in the industry of semiconductors and solar cells in China prior to his Ph.D. research. He then completed post-doctoral research at RMIT from 2017-2018. He is currently a postdoctoral researcher at the Faculty of Engineering and Natural Sciences, Tampere University (TAU),

Finland. His current research interests cover the preparation, understanding, and applications of functional nanomaterials in third generation solar cells and photocatalysis.

Paola Vivo

Paola Vivo is a University Researcher at Tampere University (TAU), Finland. After pursuing her Ph.D. in Chemistry, she received Academy of Finland fellowship for postdoctoral research in 2013–2017. She currently leads the Hybrid Solar Cells research team at TAU (Faculty of Engineering and Natural Sciences). Her research interests include developing novel organic functional materials and hybrid architectures for third generation solar cells, with current emphasis on halide perovskite photovoltaics.